

# 000 NEURAL COLLAPSE BY DESIGN: LEARNING CLASS 001 PROTOTYPES ON THE HYPERSPHERE 002

003 **Anonymous authors**

004 Paper under double-blind review

## 005 ABSTRACT

006 Neural Collapse (NC) describes the global optimum of supervised learning, yet  
007 standard cross-entropy (CE) training rarely attains its geometry in practice. This  
008 is due to unconstrained radial degrees of freedom: cross-entropy is invariant to  
009 joint rescaling of features and weights, leaving radial directions underconstrained  
010 thus preventing convergence to a unique geometry. We show that constraining op-  
011 timization to the unit hypersphere removes this degeneracy and reveals a unifying  
012 view of normalized softmax classifier learning (CL) and supervised contrastive  
013 learning (SCL) as the same prototype-contrast principle: both optimize angular  
014 similarity to class prototypes, using explicit learned weights for normalized soft-  
015 max and implicit class means for SCL. Despite this shared foundation, existing  
016 objectives suffer from small effective negative sets and interference between posi-  
017 tive and negative terms, which slows convergence to NC. We address these issues  
018 with two objectives: NTCE, which contrasts class prototypes against all batch in-  
019 stances to expand the negative set from K classes to M samples; and NONL, which  
020 normalizes only over negatives to decouple intra-class alignment from inter-class  
021 repulsion. Theoretically, we prove that SCL already learns an optimal prototype  
022 classifier under NC, eliminating the need for post-hoc typically hours-scale linear  
023 probing. Empirically, across four benchmarks including ImageNet-1K, our meth-  
024 ods surpass CE accuracy, reach  $\geq 95\%$  on NC metrics, and match NC structure  
025 with substantially fewer iterations. Moreover, SCL with class-mean prototypes  
026 matches linear-probing accuracy while requiring no training. These results re-  
027 frame supervised learning as prototype-based classification on the hypersphere,  
028 closing the theory-practice gap while simplifying training and accelerating con-  
029 vergence.

## 030 1 INTRODUCTION

031 Despite theoretical proofs that Neural Collapse (NC) is the global optimum of supervised learn-  
032 ing objectives (Lu & Steinerberger, 2022; Zhou et al., 2022a; Graf et al., 2021), standard training  
033 with cross-entropy rarely achieves this configuration in practice. This failure is particularly striking  
034 because *NC delivers precisely the properties we seek*: when neural networks do approach this geo-  
035 metric configuration, where within-class representations collapse to their means, class means form  
036 an equiangular tight frame (ETF), and classifier weights align with these prototypes, they demon-  
037 strate improved generalization (Papyan et al., 2020; Bartlett et al., 2017; Neyshabur et al., 2018),  
038 adversarial robustness (Fawzi et al., 2016; Ding et al., 2020), enhanced transfer learning (Kornblith  
039 et al., 2019; Khosla et al., 2020), and converge toward max-margin classifiers (Soudry et al., 2018)  
040 with stronger robustness guarantees (Hein & Andriushchenko, 2017). *If NC is provably optimal and*  
041 *empirically beneficial, why does standard training consistently fail to achieve it?*

042 We identify the core issue as *unconstrained radial degrees of freedom*. Cross-entropy optimization  
043 allows features and weights to be jointly rescaled without changing predictions (Soudry et al., 2018).  
044 This leaves radial directions underconstrained, preventing convergence to a unique geometry. While  
045 explicit regularization of features, weights, and biases may theoretically resolve this (Zhu et al.,  
046 2021), it introduces multiple hyperparameters that complicate practical implementation. A more  
047 principled solution is to eliminate radial freedom entirely by constraining optimization to the unit  
048 hypersphere, where NC becomes the *unique* global optimum (Yaras et al., 2022).

This geometric perspective reveals a surprising *unity* between two learning paradigms traditionally viewed as fundamentally different. Classifier learning (CL) with normalized softmax (Wang et al., 2017) has been understood as directly learning decision boundaries through weight vectors, while supervised contrastive learning (SCL) (Khosla et al., 2020) has been viewed as learning representations through instance-to-instance comparisons followed by a separate classifier training phase. We show both are actually *prototype-contrast methods on the hypersphere*: normalized softmax optimizes angular similarity between normalized features and explicit class weight vectors serving as prototypes, while SCL optimizes angular similarity among normalized instances using implicit class-mean embeddings as prototypes.

Despite this shared geometric foundation, these methods inherit computational limitations that prevent efficient NC convergence. CL suffers from a small effective negative set (denominator contrasts against only  $K$  class weights) (He et al., 2020), while both paradigms couple positive and negative similarity terms through shared normalization (Yeh et al., 2022), creating interference that slows convergence to optimal geometry. These limitations suggest that achieving NC requires not just hyperspherical constraints but also algorithmic innovations in *how prototypes are contrasted*.

Building on the insight that both paradigms are prototype-based but computationally limited, we make four five contributions:

1. We **unify normalized softmax and SCL** under a single geometric framework, revealing both as *prototype-contrast methods on the unit hypersphere* that differ only in whether prototypes are explicit (learned weights) or implicit (class means). This framework explains why both can achieve NC while standard cross-entropy cannot.
2. We propose **two supervised objectives** that overcome existing computational limitations. **NTCE** (Normalized Temperature-scaled Cross Entropy) increases the effective number of negatives from  $K$  classes to  $M$  batch samples by contrasting the class prototype against all instances in the batch, strengthening inter-class separation. **NONL** (Negatives-Only Normalization Loss) eliminates interference between intra-class alignment and inter-class repulsion by normalizing only over negatives, accelerating NC convergence.
3. We prove that *SCL already learns an optimal classifier during pretraining, eliminating the need for linear probing*. The class-mean embeddings learned by SCL form an ETF-aligned prototype classifier under NC, implementing the self-duality condition by construction and yielding equivalent accuracy without incurring the computational cost of post-training probing.
4. We validate our approach across four benchmarks including ImageNet-1K. NTCE and NONL achieve  $\geq 95\%$  on NC metrics while *surpassing standard cross-entropy accuracy*, and match cross-entropy’s NC metrics with *substantially fewer training iterations*. Our prototype classifier maintains SCL’s accuracy while eliminating hours of linear probing computation, a significant *practical saving for large-scale deployments*.
5. We empirically demonstrate that the representations learned by our objectives translate into **practical benefits**, yielding improved performance on *transfer learning* (e.g., +5.5% mean relative improvement), *long-tailed classification* (up to +8.7% relative improvement), and *robustness* (lower mCE).

These results suggest a **fundamental shift** in how supervised learning should be understood: not as unconstrained optimization in Euclidean space, but as *prototype-based classification on the hypersphere*. By making this geometry explicit, we close the theory-practice gap, simplify training, accelerate convergence, and yield interpretable models that provably realize their optimal NC structure. The *practical impact is substantial*: faster training, elimination of extra compute phases, and models that reach the theoretical optimum. The *theoretical insight* provides a principled foundation for future advances in supervised learning.

## 2 RELATED WORK

**Neural Collapse.** Neural Collapse (NC) describes a limiting geometry in which within-class features collapse to their means (NC1), class means form a centered simplex ETF (NC2), classifier weights align with the means (NC3), and biases collapse (NC4) (Papyan et al., 2020). Variants of

108 this structure characterize global minimizers for several objectives and modeling assumptions, in-  
 109 cluding MSE (Han et al., 2022; Zhou et al., 2022a), cross-entropy (CE) (Lu & Steinerberger, 2022),  
 110 supervised contrastive learning (SCL) (Graf et al., 2021), and CE variants such as label smoothing  
 111 and focal loss (Zhou et al., 2022b). In finite training, however, standard CE with weight decay often  
 112 fails to realize the optimal geometry: the loss is *scale-noncoercive* and can be driven toward zero by  
 113 inflating logit magnitudes without improving angular structure (Albert & Anderson, 1984; Soudry  
 114 et al., 2018). Class imbalance further distorts the ETF and slows convergence (Thrampoulidis et al.,  
 115 2022; Hong & Ling, 2024); free bias terms obstruct NC4 and can exacerbate miscalibration unless  
 116 controlled (e.g., logit adjustment) (Menon et al., 2021). While simultaneously penalizing features,  
 117 weights, and biases can restore coercivity and yield NC in principle (Zhu et al., 2021; Zhou et al.,  
 118 2022a), tuning multiple regularizers is brittle. *We show that contrasting instances against class*  
 119 *prototypes on the hypersphere operationalizes NC in practice.*

120 **Learning on the hypersphere.** Constraining radial freedom is a principled route to NC. When  
 121 both features and classifier lie on the unit hypersphere, CE over the product of spheres exhibits a  
 122 benign strict-saddle landscape whose minima realize perfect NC (Yaras et al., 2022). Related evi-  
 123 dence appears in contrastive objectives: SCL yields within-class collapse and simplex class means  
 124 (Graf et al., 2021), while in self-supervised contrastive learning batch-level optima form a simplex  
 125 ETF (Koromilas et al., 2024). A long line of face-recognition work, including SphereFace, CosFace,  
 126 ArcFace, and NormFace (Liu et al., 2017; Wang et al., 2018; Deng et al., 2019; Wang et al., 2017),  
 127 operationalizes direction-only discrimination by using angular/cosine margins. *We unify these ap-*  
 128 *praches by showing that both normalized softmax and SCL perform prototype contrast on the hy-*  
 129 *persphere.* Building on this bridge, we extend normalized softmax with NTCE/NONL to import  
 130 desirable properties.

131 **Prototype-based classification and ETF classifiers.** Prototype methods classify via distances to  
 132 learned representatives (Snell et al., 2017). Motivated by NC, several works fix or guide the clas-  
 133 sifier toward ETF-like prototypes and learn only the encoder, for example by (i) fixing a simplex  
 134 ETF head and training the backbone (ETF+DR) (Yang et al., 2022), (ii) using hyperspherical proto-  
 135 type networks (Mettes et al., 2019), or (iii) constructing equiangular basis vectors (EBVs) (Shen  
 136 et al., 2023). Other approaches enforce (non-negative) orthogonality (Kim & Kim, 2024) or guide  
 137 the classifier toward the nearest ETF via a Riemannian inner optimization (Markou et al., 2024).  
 138 Recently NC structure has been exploited in a teacher–student setting (Zhang et al., 2025): given a  
 139 trained teacher that already exhibits NC, they compute *teacher* class centroids and use them as an  
 140 NC3-inspired classifier for the *student*. *Our perspective is that CL and SCL already operate with*  
 141 *prototypes: we modify the objectives to realize NC in practice, and we show that SCL’s class-mean*  
 142 *prototypes form an effective classifier, making linear probing unnecessary.*

### 3 PRELIMINARIES

145 **Notation.** Scalars are denoted by lowercase letters  $u$ , vectors by lowercase bold letters  $\mathbf{u}$ , and mat-  
 146 rices by uppercase bold letters  $\mathbf{U}$ . Sets are represented by uppercase caligraphic letters  $\mathcal{U}$ . Individual  
 147 elements are accessed using subscript notation:  $u_i$  for the  $i$ -th element of vector  $\mathbf{u}$  and  $U_{i,j}$  for the  
 148 element at row  $i$  and column  $j$  of matrix  $\mathbf{U}$ . To denote vertical (row-wise) concatenation of matrices  
 149  $\mathbf{X}$  and  $\mathbf{Y}$ , we use  $[\mathbf{X}; \mathbf{Y}]$ . We denote normalized vectors with  $\hat{\mathbf{u}}_j = \mathbf{u}_j / \|\mathbf{u}_j\|$ .

#### 3.1 LEARNING PARADIGMS

152 **Classifier Learning with Cross-Entropy.** The cross-entropy loss is the standard Classifier Learning  
 153 (CL) objective, optimizing representations and classifier weights simultaneously. An encoder  $f_{\theta} :  
 154 \mathcal{X} \rightarrow \mathcal{Z}$ , parameterized by  $\theta \in \Theta$ , maps an input  $\mathbf{x} \in \mathcal{X}$  to its representation  $\mathbf{z} = f_{\theta}(\mathbf{x}) \in \mathcal{Z}$ . For a  
 155  $K$ -class task,  $y_i$  denotes the class assignment of sample  $\mathbf{x}_i$ . A linear classifier is placed on top of the  
 156 encoder, with weight matrix  $\mathbf{W} \in \mathbb{R}^{K \times h}$  and bias  $\mathbf{b} \in \mathbb{R}^K$ , where  $h$  is the embedding dimension.  
 157 For a mini-batch of  $M$  samples with  $\{\mathbf{z}_i\}_{i=1}^M$ , the cross-entropy loss is defined as

$$\mathcal{L}_{\text{CE}}(\mathbf{Z}, \mathbf{W}) = \frac{1}{M} \sum_{i=1}^M -\log \left( \frac{e^{\mathbf{z}_i^\top \mathbf{w}_{y_i} + b_{y_i}}}{\sum_{j=1}^K e^{\mathbf{z}_i^\top \mathbf{w}_j + b_j}} \right), \quad (1)$$

158 where  $\mathbf{w}_j$  denotes the  $j$ -th row of  $\mathbf{W}$  and  $b_j$  the  $j$ -th component of  $\mathbf{b}$ .

**Supervised Contrastive Learning.** *Supervised Contrastive Learning (SCL)* takes a seemingly different direction: it learns representations by exploiting similarities between instances to learn class-invariant representations. Building on our notation, the contrastive framework augments the encoder  $f_\theta : \mathcal{X} \rightarrow \mathcal{Z}$  with a projection head  $g_\phi : \mathcal{Z} \rightarrow \mathcal{U}$ , parameterized by  $\phi \in \Phi$ , which maps representations onto the unit hypersphere,  $\mathcal{U} = \mathbb{S}^{d-1} = \{\mathbf{u} \in \mathbb{R}^d \mid \|\mathbf{u}\| = 1\}$ . We denote the projected representations as  $\mathbf{u}, \mathbf{v} \in \mathcal{U}$ , where  $\mathbf{u}_i$  comes from instance  $\mathbf{x}_i$  and  $\mathbf{v}_i$  from its alternative view produced via augmentation, a typical process in contrastive learning.

For SCL the objective is to pull together positive pairs while pushing apart negative pairs in the projection space. Typically alternative views of the same data point that originate from augmentation are considered as new data points, *i.e.*  $\mathbf{A} = [\mathbf{U}; \mathbf{V}]$ , and the supervised contrastive loss becomes:

$$\mathcal{L}_{\text{SCL}}(\mathbf{A}) = \frac{1}{2M} \sum_{i=1}^{2M} -\frac{1}{|\mathcal{C}(i)|} \sum_{l \in \mathcal{C}(i)} \log \left( \frac{e^{\mathbf{a}_i^\top \mathbf{a}_l / \tau}}{\sum_{\substack{j=1 \\ j \neq i}}^{2M} e^{\mathbf{a}_i^\top \mathbf{a}_j / \tau}} \right), \quad (2)$$

where  $\mathcal{C}(i)$  denotes the set of indices corresponding to positive examples sharing the same class as  $\mathbf{x}_i$  and  $\tau > 0$  is a temperature parameter that controls the concentration of the distribution.

A crucial distinction emerges post-training: while learning with cross-entropy directly produces a classifier, contrastive learning requires an additional step. After optimizing Equation (2), the projection head is discarded and a linear classifier  $\mathbf{W}, \mathbf{b}$  is trained on the frozen encoder representations  $\mathbf{z}$  using Equation (1), a process known as **linear probing**.

### 3.2 NEURAL COLLAPSE (NC).

**Neural Collapse** Papyan et al. (2020) is the late-training regime (on balanced data) where last-layer features and the linear classifier converge to a highly structured limit. Let  $\mathbf{z}_i = f(\mathbf{x}_i) \in \mathbb{R}^h$ , class means  $\boldsymbol{\mu}_c = \frac{1}{n_c} \sum_{i:y_i=c} \mathbf{z}_i$ , weights  $\mathbf{w}_c$ , and bias  $\mathbf{b}$ . NC holds when, up to common scalings:

(NC1) **Within-class collapse:**  $\mathbf{z}_i = \boldsymbol{\mu}_{y_i}$  for all  $i$ .

(NC2) **Simplex ETF of class means:** the centered means  $\tilde{\boldsymbol{\mu}}_c = \boldsymbol{\mu}_c - \frac{1}{K} \sum_{k=1}^K \boldsymbol{\mu}_k$  have equal norms and equal pairwise angles so the means span a centered  $(K-1)$ -simplex ETF.

(NC3) **Alignment of Class Representation and Classifier:** classifier columns align with the class means,  $\mathbf{w}_c \parallel \boldsymbol{\mu}_c$  (there exists  $\gamma > 0$  with  $\mathbf{w}_c = \gamma \boldsymbol{\mu}_c$ ).

(NC4) **Bias collapse:**  $\mathbf{b} = \beta \mathbf{1}$  for some scalar  $\beta$ .

Under NC, the decision rule reduces to nearest-class-mean classification. We assume balanced classes and  $h \geq K - 1$  so a centered simplex ETF is feasible (Lu & Steinerberger, 2022).

**Practical Challenges in reaching Neural Collapse** Neural Collapse (NC) is now well documented in deep nets (Papyan et al., 2020) and characterizes global minima of balanced cross-entropy (Lu & Steinerberger, 2022). However standard pipelines does not enforce it in practice. For the typical paradigm of cross-entropy and classifier weight decay, the objective admits an *unbounded rescaling direction*: shrinking the classifier while amplifying features leaves logits unchanged, reduces the penalty, and drives the loss toward zero without achieving NC (Soudry et al., 2018; Albert & Anderson, 1984). It is shown by Zhu et al. (2021) that a well-posed objective arises when all radial degrees of freedom are constrained by penalizing weights, features, and biases simultaneously (Zhu et al., 2021). However this is practically brittle due to multiple regularizers to tune.

Supervised contrastive training on the other hand can drive representations toward NC geometry (Graf et al., 2021). However, the subsequent *linear probing* step typically fits a softmax classifier with cross-entropy on *frozen* features, allowing free weight magnitudes and biases. This reintroduces the same scale and bias pathologies as cross-entropy even when training has already reached an NC.

## 4 SUPERVISED LEARNING ON THE HYPERSPHERE

In this section we present a common view-point bridging classifier learning and contrastive learning to accelerate neural collapse. Our approach leverages similarity-based optimization while elimi-

216 nating radial degrees of freedom by constraining both feature and classifier norms to the hyper-  
 217 sphere. This constraint transforms the optimization landscape into a benign geometry where all  
 218 critical points become global optima (Yaras et al., 2022), enabling direct convergence to NC.  
 219

#### 220 4.1 REVISITING CROSS ENTROPY: CONTRASTING CLASS PROTOTYPES TO INSTANCES 221

222 The weight matrix of the final linear classifier in CL methods can be expressed as  $\mathbf{W} =$   
 223  $[\mathbf{w}_1; \mathbf{w}_2; \dots; \mathbf{w}_K] \in \mathbb{R}^{K \times h}$ , where each  $\mathbf{w}_c$  represents a learnable class prototype. This formu-  
 224 lation reveals an important insight: we can treat the classifier weights as *learnable prototypes* that  
 225 evolve through gradient descent to capture class-specific geometric structures. Building on this we  
 226 design objectives that leverage such prototypes to help arrive at the optimal NC geometry.  
 227

228 **Normalized Softmax Losses.** Standard cross-entropy and contrastive learning represent two seem-  
 229 ingly distinct paradigms: the former discriminates through learned magnitudes and biases in un-  
 230 constrained space, while the latter operates purely on angular similarities on the hypersphere. This  
 231 fundamental difference leads to a critical inefficiency: while both methods theoretically converge to  
 232 neural collapse configurations, cross-entropy introduces unnecessary radial degrees of freedom that  
 233 slow convergence to this optimal geometry (Yaras et al., 2022; Zhu et al., 2021).  
 234

235 Normalized softmax losses resolve this inefficiency by reformulating cross-entropy as a pure geo-  
 236 metric objective. NormFace (Wang et al., 2017), a prominent example, achieves this through  
 237 three coordinated modifications: (i) eliminating biases that merely translate decision boundaries  
 238 without encoding semantic structure, (ii) projecting representations onto the hypersphere to focus  
 239 exclusively on angular geometry, and (iii) introducing temperature scaling to control concentration  
 240 of the softmax distribution. Formally, with  $\mathbf{u}_i = \mathbf{z}_i / \|\mathbf{z}_i\|_2$  as the normalized representation and  
 241  $\hat{\mathbf{w}}_j = \mathbf{w}_j / \|\mathbf{w}_j\|_2$  as the normalized classifier weight for class  $j$ , NormFace minimizes:  
 242

$$243 L_{\text{NormFace}}(\mathbf{U}, \mathbf{W}) = -\frac{1}{M} \sum_{i=1}^M \log \left( \frac{e^{\mathbf{u}_i^\top \hat{\mathbf{w}}_{y_i} / \tau}}{\sum_{j=1}^K e^{\mathbf{u}_i^\top \hat{\mathbf{w}}_j / \tau}} \right). \quad (3)$$

244 This reformulation transforms classification into contrastive learning between data instances and  
 245 learnable class prototypes while maintaining cross-entropy’s computational efficiency.  
 246

#### Normalized Temperature-scaled Cross Entropy (NTCE)

247 When utilizing NormFace to view CL from a contrastive learning perspective we end up with an  
 248 inherent limitation of cross entropy: the number of negatives in the objective is limited to  $K$ , the  
 249 number of class prototypes. It is very well investigated that contrastive objectives need very large  
 250 numbers of negatives in order to converge (He et al., 2020). This is mostly due to the fact that fewer  
 251 negatives provide a worse estimate to the expectation of the actual contrastive objective (Koromilas  
 252 et al., 2024).  
 253

254 By inverting the contrastive direction from instance-to-class to class-to-instance discrimination we  
 255 address this limitation through the Normalized Temperature-scaled Cross Entropy (NTCE). This  
 256 modification fundamentally alters the learning dynamics: rather than each instance contrasting  
 257 against  $K$  class prototypes, each class prototype now contrasts against  $M$  batch representations.  
 258

259 The key insight underlying NTCE is that *class prototypes themselves can serve as anchors* in the  
 260 contrastive formulation. By anchoring on the class weight vector corresponding to each instance’s  
 261 ground-truth label and contrasting it against all batch representations, we dramatically expand the  
 262 negative sampling space. Formally, NTCE takes the form:  
 263

$$264 L_{\text{NTCE}}(\mathbf{U}, \mathbf{W}) = \frac{1}{M} \sum_{i=1}^M -\log \left( \frac{e^{\hat{\mathbf{w}}_{y_i}^\top \mathbf{u}_i / \tau}}{\sum_{j=1}^M e^{\hat{\mathbf{w}}_{y_i}^\top \mathbf{u}_j / \tau}} \right), \quad (4)$$

265 where  $\hat{\mathbf{w}}_{y_i}$  serves as the anchor for instance  $i$ , and critically, the denominator sums over all  $M$   
 266 instances in the batch rather than over  $K$  classes.  
 267

268 **Negatives Only Normalization Loss.** NTCE adds enhanced negative sampling on top of NormFace  
 269 to directly transfer the principles of contrastive learning to cross entropy training. However, it also  
 270 brings a fundamental drawback of popular contrastive objectives that compromises its optimization  
 271 dynamics. The denominator in Equation (4) indiscriminately aggregates all instances sharing the  
 272

same class anchor. That is the denominator, also known as the uniformity term, is optimized when instances of the same class have maximum distance (Wang & Isola, 2020), which contradicts the optimality of the numerator (alignment terms). More specifically, positive pairs explicitly appear as negative samples in the normalization term, generating gradients that actively repel instances from their own class prototype. When instance  $i$  and instance  $j$  share class  $y_i = y_j$ , the term  $e^{\hat{\mathbf{w}}_{y_i}^\top \mathbf{u}_j / \tau}$  in the denominator produces gradients that decrease  $\hat{\mathbf{w}}_{y_i}^\top \mathbf{u}_j$ , directly opposing the alignment objective. This is a known behavior that is called *alignment-uniformity coupling* (Yeh et al., 2022).

In order to resolve this conflict we introduce the Negatives-Only Normalization Loss (NONL), which explicitly excludes same-class instances from the denominator:

$$L_{\text{NONL}}(\mathbf{U}, \mathbf{W}) = \frac{1}{M} \sum_{i=1}^M -\log \left( \frac{e^{\hat{\mathbf{w}}_{y_i}^\top \mathbf{u}_i / \tau}}{\sum_{\substack{j=1 \\ j \notin \mathcal{C}(i)}}^M e^{\hat{\mathbf{w}}_{y_i}^\top \mathbf{u}_j / \tau}} \right). \quad (5)$$

**NC optimality of normalized objectives.** In Theorem 4.1 we show that, in the balanced UFM/LPM setting (Tirer & Bruna, 2022; Yaras et al., 2022), the three normalized losses (NormFace, NTCE, and NONL) are globally optimized by Neural Collapse (NC) geometry. The proof is deferred to Section A.1 and proceeds via a unified three-step reduction for NTCE and NONL: (i) we reduce the sample-level losses to class-mean based objectives using Jensen’s inequality with explicit tightness conditions, (ii) we show these class-level objectives are contrastive losses whose global minimizers exhibit a centered simplex ETF structure where class-means align with the classifier, and (iii) we invoke the tightness conditions to prove any global minimizer must collapse each class to a single feature vector, recovering NC at the sample level. For NormFace, we establish an exact equivalence with the constrained UFM formulation of Yaras et al. (2022), directly invoking their Neural Collapse theorem.

**Theorem 4.1** (Neural Collapse optimality of normalized losses). *In the balanced UFM/LPM setting above with  $d \geq K$ , every global minimizer of  $\mathcal{L}_{\text{NF}}$ ,  $\mathcal{L}_{\text{NTCE}}$ , and  $\mathcal{L}_{\text{NONL}}$  satisfies NC1–NC3 (within-class collapse, simplex ETF class means, and classifier–feature alignment), up to a global rotation and permutation of class labels.*

## 4.2 REVISITING SUPERVISED CONTRASTIVE LEARNING: CONTRASTING MEAN-CLASS PROTOTYPES TO INSTANCES

**SCL implicitly learns prototype classifiers.** We follow Equation (2) to treat alternative views produced by data augmentation as distinct samples, i.e.,  $\mathbf{A} = [\mathbf{U}; \mathbf{V}]$ . Let  $\mathcal{B}_c = \{j \in [2M] : y_j = c\}$  denote the within-batch index set for class  $c$ ,  $n_c = |\mathcal{B}_c|$ , and  $\hat{\mathbf{\mu}}_c = \frac{1}{n_c} \sum_{j \in \mathcal{B}_c} \mathbf{a}_j$  the corresponding batch prototype (class mean). We define the *prototype loss*:

$$L_{\text{proto}}(\mathbf{A}) = -\frac{1}{2M} \sum_{i=1}^{2M} \log \left( \frac{e^{\mathbf{a}_i^\top \hat{\mathbf{\mu}}_{y_i} / \tau}}{-e^{\mathbf{a}_i^\top \hat{\mathbf{\mu}}_{y_i} / \tau} + \sum_{c=1}^K n_c \cdot e^{\mathbf{a}_i^\top \hat{\mathbf{\mu}}_c / \tau}} \right), \quad (6)$$

where the numerator encourages alignment with the correct class prototype, while the denominator includes both positive and negative prototypes weighted by their batch frequencies  $n_c$ . Theorem 4.2 connects the optima of this loss to the ones of SCL. The proof can be found in Section A.2.

**Theorem 4.2** (Equivalence of SCL and prototype–softmax minimizers). *For unit-norm representations and balanced labels the supervised contrastive loss  $L_{\text{SCL}}$  and the prototype loss  $L_{\text{proto}}$  in Equation (6) share the same set of global minimizers (up to rotation and label permutation). In particular, at every global minimizer the representations exhibit in-class collapse and the class means form a centered simplex ETF.*

This result clarifies our understanding of SCL: rather than merely learning good representations for classification, SCL directly optimizes for classifier–feature alignment through its contrastive objective. The learned prototypes are not just byproducts but the optimal classifiers themselves.

**Connection to Classifier Learning.** The  $n_c$  weighting in the denominator of Equation (6) captures the effect of utilizing multiple negative instances, matching the structure of Equation (4). When discarding the  $n_c$  weights, this loss reduces to Equation (3), establishing a direct **correspondence**

324 Table 1: Performance comparison of learning paradigms and objectives across datasets. **Bold**: best  
 325 within method family; **green**: overall best per dataset.

(I) Classifier Learning Methods					
Loss	CIFAR-10	CIFAR-100	ImageNet-100	ImageNet-1K	
CE	94.6	72.1	84.4	75.4	
ETF + DR	94.4	72.1	84.5	75.4	
NORMFACE	94.8	72.4	84.4	76.4	
NTCE (ours)	94.7	72.9	84.7	<b>76.7</b>	
NONL (ours)	<b>94.9</b>	<b>73.6</b>	<b>84.9</b>	76.5	

(II) Supervised Contrastive Learning Methods						
Classifier Learning	Loss	Forward Passes	CIFAR-10	CIFAR-100	ImageNet-100	ImageNet-1K
LINEAR PROBING	SCL	$T \times N$	<b>95.0</b>	<b>73.9</b>	84.8	<b>75.1</b>
NORMALIZED LINEAR PROBING	SCL	$T \times N$	94.9	73.6	84.8	<b>75.1</b>
FIXED PROTOTYPES	SCL	<b>N</b>	<b>95.0</b>	<b>73.9</b>	<b>86.8</b>	<b>75.1</b>

343 **between the prototype weights and class means.** Adding that the optimal solution of Equation (3)  
 344 holds when  $w_c = \hat{\mu}_c$  (Yaras et al., 2022) the connection becomes even more prevalent.

345 In other words, despite SCL converging to collapsed class representations forming an ETF, its optima  
 346 can also be attained by contrasting instances to class-mean prototypes. This connects CL techniques  
 347 to SCL, where the learnable classifier weights in the former are free parameters while in the latter  
 348 they emerge implicitly from the learned representations.

349 **Why linear probing fails for SCL features.** In practice linear probing is used to train a classifier for  
 350 the learned SCL representations. This approach introduces **unnecessary degrees of freedom** that  
 351 disrupt the geometric optimality achieved by SCL. Specifically this process introduces: (i) **geometric  
 352 mismatch**: SCL features live on the hypersphere with collapsed, ETF-structured class means.  
 353 Linear probing operates in unconstrained Euclidean space, allowing weight rescaling and bias shifts  
 354 that break classifier-feature alignment (Soudry et al., 2018). (ii) **Redundancy**: Our theorem shows  
 355 SCL has already learned optimal classifier weights, *i.e.* the class prototypes themselves.

356 **Class-mean Prototypes inplace of Linear Probing.** We observe that class prototypes  $\hat{\mu}_c$  serve as  
 357 natural classifier weights that satisfy NC3 (classifier-feature alignment) by construction. Rather than  
 358 retrofitting a linear head to pre-collapsed features, we directly impose the NC-optimal classifier from  
 359 the learned geometry. We *discard linear probing entirely* and set the classifier weights to the learned  
 360 prototypes:  $w_c = \hat{\mu}_c$ . Doing so, we alleviate the need for an extra training phase, and we show  
 361 empirically (Section 5) that this prototype-based classification matches linear probing performance.

## 363 5 EXPERIMENTS

365 In this section we empirically validate our methods against cross-entropy (CE), ETF + DR (Yang  
 366 et al., 2022), and NormFace(Wang et al., 2017) for Classifier Learning paradigms and supervised  
 367 contrastive learning (SCL), evaluating: (i) classification accuracy, (ii) proximity to neural collapse  
 368 geometry, and (iii) NC convergence speed. Experiments are conducted on four standard datasets:  
 369 *CIFAR10*, *CIFAR100*, *ImageNet-100*, and *ImageNet1K*, following common representation learning  
 370 benchmarking practices (Khosla et al., 2020; Markou et al., 2024; Wang et al., 2021; Yeh et al.,  
 371 2022). We use ResNet50 for ImageNet datasets and ResNet18 for CIFAR. Implementation details  
 372 are provided in Section A.3.

### 374 5.1 CLASSIFICATION PERFORMANCE

375 **Classifier Learning Methods.** As can be inferred from Table 1(I), normalized losses *outperform*  
 376 *cross-entropy* (CE) in all cases, while also our losses further outperform NormFace. NONL achieves  
 377 the strongest gains on datasets with few (10) to medium (100) number of classes while it has the

378 second best score on ImageNet-1K. Here we have to note that ImageNet-1K, our objectives exhibit  
 379 the typical behavior of contrastive-style objectives: they benefit from larger batch sizes, whereas  
 380 using smaller batches leads to degraded performance due to insufficient in-batch negatives (see  
 381 Section A.5).

382 **Supervised Contrastive Learning Methods.** The accuracy from three classifier learning strategies  
 383 on SCL representations is presented in Table 1(II): (i) standard linear probing with learnable weights  
 384 and bias, (ii) normalized linear probing using NormFace loss, and (iii) fixed prototypes computed  
 385 as class-mean embeddings. Fixed prototypes match linear probing performance on 3 of 4 datasets,  
 386 and mark a considerable +2.0% improvement on ImageNet-100 **requiring only  $N$  forward passes**  
 387 **versus**  $T \times N$  for training-based methods, where  $T$  is the number of epochs. Normalized linear  
 388 probing achieves comparable accuracy to standard linear probing, validating that the *discriminative*  
 389 *information in SCL features resides primarily in their angular structure* rather than magnitude or  
 390 biases. These findings validate that angular structure alone suffices for discrimination in well-trained  
 391 representations, enabling *training-free classification* in SCL via fixed prototypes that **eliminate huge**  
 392 **computational costs** by discarding a, typically hours long, training phase.

## 393 5.2 QUANTIFYING NEURAL COLLAPSE

395 We quantify NC1–NC3 with complementary, condition-specific metrics; we omit NC4 (bias col-  
 396 lapsed) as our models enforce zero bias by design.

398 **Effective Rank (NC1, NC2).** For matrix  $\mathbf{A}$  with singular values  $\{\sigma_i\}$  the effective rank (Roy &  
 399 Vetterli, 2007) is defined as  $\text{erank}(\mathbf{A}) = \exp\{-\sum_i p_i \log p_i\}$  where  $p_i = \sigma_i / \sum_j \sigma_j$ . We compute  
 400 the intra and inter class effective ranks (Zhang et al., 2024) as:  $\text{erank}_{\text{intra}} = \frac{1}{K} \sum_{c=1}^K \text{erank}(\text{Cov}[\mathbf{z}_i -$   
 401  $\mu_c \mid y_i = c])$  and  $\text{erank}_{\text{inter}} = \text{erank}(\text{Cov}[\mu_c - \mu_G])$ , where Cov is the covariance matrix. These  
 402 metrics quantify **NC1** (within-class variability collapse):  $\text{erank}_{\text{intra}} \rightarrow 0$  indicates  $\mathbf{z}_i \rightarrow \mu_{y_i}$ , and  
 403 **NC2** (ETF structure): Zhang et al. (2024) proved that when  $\text{erank}_{\text{inter}} = K - 1$  the class means form  
 404 a simplex with equal pairwise angles. We also report  $\text{erank}(\mathbf{W})$  to assess whether classifier weights  
 405 approximate an equiangular tight frame (ETF).

406 **Alignment (NC3).** We quantify feature–classifier alignment by  $\frac{1}{N} \sum_{i=1}^N \|\mathbf{z}_i - \mathbf{w}_{y_i}\|_2^2$  and also report  
 407 instance-to-instance alignment to probe per-class collapse.

408 **Information Metrics (NC2, NC3).** For normalized Gram matrices  $\mathbf{G}_W$  (weights),  $\mathbf{G}_M$  (class  
 409 means) and  $\mathbf{H}$  being the matrix entropy, Song et al. (2024) connects Neural Collapse to the metrics:

$$411 \text{MIR} = \frac{\mathbf{H}(\mathbf{G}_W) + \mathbf{H}(\mathbf{G}_M) - \mathbf{H}(\mathbf{G}_W \odot \mathbf{G}_M)}{\min\{\mathbf{H}(\mathbf{G}_W), \mathbf{H}(\mathbf{G}_M)\}}, \quad \text{HDR} = \frac{|\mathbf{H}(\mathbf{G}_W) - \mathbf{H}(\mathbf{G}_M)|}{\max\{\mathbf{H}(\mathbf{G}_W), \mathbf{H}(\mathbf{G}_M)\}} \quad (7)$$

413 These capture the information-theoretic signatures of **NC2** and **NC3** where under full collapse  
 414 MIR  $\rightarrow 1$  and HDR  $\rightarrow 0$ , reflecting perfect structural alignment.

416 In Table 2 four key findings are revealed: **(i) CE fails to achieve NC:** high intra-class variance (er-  
 417 ank 22.5/96.4), suboptimal inter-class separation (erank 8.6/57.1 vs. theoretical K-1=9/99), and  
 418 poor weight-feature alignment (w-inst 0.59/0.83, inst-inst 0.69/1.05). **(ii) Normalized softmax**  
 419 **losses satisfy NC2-NC3** since they achieve perfect inter-class separation (erank 9.0/99.0), near-zero  
 420 alignment errors (NTCE: w-inst 0.08/0.01, inst-inst 0.10/0.05), and optimal weight dimensional-  
 421 ity matching the simplex ETF, with **NONL being the overall best** mostly due to its better intra  
 422 class structure. **(iii) SCL with linear probing violates NC3:** despite superior within-class collapse  
 423 (erank 4.5/7.5), inter-class structure degrades (erank 9.0/66.7) and classifier-feature alignment fails  
 424 (w-inst 0.99/1.03). **(iv) Fixed prototypes restore NC3 in SCL:** removing the trainable classifier  
 425 enforces perfect alignment by construction, though inter-class separation remains suboptimal.

426 While CE and ETF+ DR attain slightly better MIR/HDR values than our normalized losses, these  
 427 information-theoretic metrics primarily reflect the overall entropy/redundancy of the representation,  
 428 not the NC geometry itself. In our case, CE appears to preserve a bit more raw variability, but  
 429 organizes it in a less NC-like, less prototype-structured way (higher intra-class effective rank, weaker  
 430 alignment), whereas our normalized losses reshape the same information into a cleaner NC geome-  
 431 try. As our downstream experiments show in Section 5.3, this structured organization is more ben-  
 432 efitical for transfer, long-tailed performance, and robustness, even though CE may capture slightly  
 433 more “information” by these metrics.

432 Table 2: NC metrics on CIFAR-10/100 (training). **Bold** marks the best within each learning family;  
 433 **green** marks the overall best per dataset. Theoretical optima: Intra ER 0/0, Inter ER 9/99, Weights  
 434 ER 9/99, Weight Align 0/0, Instance Align 0/0, MIR 1/1, HDR 0/0.

436 Learning Family	437 Method	438 Effective Rank			439 Alignment		440 Information Theory Metrics	
		441 Intra ↓	442 Inter ↑	443 Weights ↑	444 Weight ↓	445 Instance ↓	446 MIR ↑	447 HDR ↓
448 CLASSIFIER 449 LEARNING	450 CE	22.5 / 96.4	8.6 / 57.1	8.9 / 89.7	0.59 / 0.83	0.69 / 1.05	<b>0.98</b> / 0.97	0.03 / 0.13
	451 ETF + DR	9.00 / 18.4	8.90 / 94.8	<b>9.00</b> / <b>99.00</b>	0.58 / 0.59	0.59 / 0.61	<b>0.98</b> / <b>1.00</b>	<b>0.02</b> / <b>0.11</b>
	452 NormFace	10.5 / 13.6	<b>9.0</b> / 96.2	<b>9.0</b> / 96.1	0.12 / <b>0.01</b>	0.14 / 0.06	0.95 / <b>1.00</b>	0.04 / 0.30
	453 NTCE	9.0 / 12.6	<b>9.0</b> / <b>99.0</b>	8.9 / 98.9	<b>0.08</b> / <b>0.01</b>	<b>0.10</b> / <b>0.05</b>	0.96 / <b>1.00</b>	0.05 / 0.30
	454 NONL	<b>4.0</b> / <b>11.4</b>	<b>9.0</b> / <b>99.0</b>	<b>9.0</b> / <b>99.0</b>	0.11 / <b>0.01</b>	0.16 / 0.06	0.95 / <b>1.00</b>	0.05 / 0.30
455 CONTRASTIVE 456 LEARNING	457 SCL (w probing)	<b>4.5</b> / <b>7.5</b>	<b>9.0</b> / <b>66.7</b>	8.3 / <b>77.8</b>	0.99 / 1.03	<b>0.10</b> / <b>0.34</b>	0.99 / <b>0.95</b>	<b>0.07</b> / <b>0.11</b>
	458 SCL (w/o probing)	<b>4.5</b> / <b>7.5</b>	<b>9.0</b> / <b>66.7</b>	<b>9.0</b> / 66.5	<b>0.00</b> / <b>0.00</b>	<b>0.10</b> / <b>0.34</b>	<b>1.00</b> / 0.87	0.09 / 0.14

448 Table 3: Convergence speed (% of training iters): (I) time to reach the 95% NC threshold; (II) time  
 449 to match CE’s final value; “0%” indicates the target is met at the first logged eval.

450 Method	451 Instance alignment	452 Weight alignment	453 Weights erank	454 Intra erank	455 Inter erank
<b>(I) NC convergence to 95% threshold (ratio to max iterations)</b>					
456 NormFace	<b>79.4%</b>	8.2%	52.6%	45.4%	56.2%
457 NTCE	<b>79.4%</b>	<b>6.8%</b>	56.4%	36.6%	52.4%
458 NONL	<b>79.4%</b>	7.4%	<b>34.6%</b>	<b>14.6%</b>	<b>47.2%</b>
<b>(II) CE convergence to converged value (ratio to CE converged iteration)</b>					
459 NormFace	<b>2.2%</b>	2.0%	66.3%	0%	7.4%
460 NTCE	<b>2.2%</b>	<b>1.8%</b>	73.9%	0%	7.4%
461 NONL	<b>2.2%</b>	<b>1.8%</b>	<b>35.4%</b>	0%	<b>6.0%</b>

462 **Convergence Dynamics.** On CIFAR-100, we track NC metrics and define convergence as the  
 463 earliest iteration where the exponentially-weighted moving average enters and remains within a  
 464 metric-specific tolerance around the 95% NC threshold.

465 In Table 3(I) the convergence speed to 95% of theoretical NC thresholds is quantified. Normalized  
 466 losses reach these thresholds, *typically early in training*. NONL converges faster with **gains**  
 467 over **NormFace for the rank metrics** (1.2-3.1 speedup), benefiting from simplified optimization  
 468 without competing terms. Table 3(II) benchmarks against CE’s converged values. The acceleration  
 469 is dramatic: normalized losses reach CE-equivalent values in under 7.5% of CE’s required iterations  
 470 across 4/5 metrics, while **NONL converges faster**. This demonstrates that normalized losses  
 471 fundamentally restructure the optimization landscape, *enabling direct paths to neural collapse*.

### 472 5.3 PRACTICAL BENEFITS OF COLLAPSED REPRESENTATIONS

473 **Transfer learning.** We first ask whether representations that lie closer to the NC regime are more  
 474 generalizable to unseen tasks. Following typical pipelines (Khosla et al., 2020), we freeze the pre-  
 475 trained encoder for each loss and train a linear classifier (or detection head for VOC07) on eight  
 476

477 Table 4: Transfer learning results. Numbers are top-1 accuracy (%) for all datasets except VOC2007  
 478 (mAP). Best per column in **green**. The last row reports NONL’s relative improvement over CE.

480 Method	481 Food	482 CIFAR10	483 CIFAR100	484 Cars	485 DTD	486 Pets	487 Flowers	488 VOC2007	489 Mean
490 CE	68.0	88.6	67.7	25.9	69.9	67.0	81.4	67.1	<b>67.0</b>
491 ETF + DR	57.2	83.9	54.3	9.8	64.0	49.2	58.3	60.0	<b>54.6</b>
492 NormFace	69.8	89.8	69.7	29.7	<b>70.1</b>	69.7	83.2	67.9	<b>68.7</b>
493 NTCE	69.3	89.9	69.8	28.1	70.0	69.4	81.9	67.8	<b>68.3</b>
494 NONL	<b>70.7</b>	<b>90.0</b>	<b>71.0</b>	<b>38.1</b>	69.4	<b>72.9</b>	<b>85.2</b>	<b>68.3</b>	<b>70.7</b>
495 $\Delta(\text{NONL-CE})$ +4.0% +1.6% +4.9% +47.1% -0.7% +8.8% +4.7% +1.8% +5.5%									

486  
487  
488  
489 Table 5: Performance under class imbalance on CIFAR-10-LT/100-LT vs. imbalance ratio  $\tau$  (Yang  
490 et al., 2022). Best per column in **green**; last row shows NONL’s relative improvement over CE.  
491  
492  
493  
494  
495  
496

Method	CIFAR-10-LT			CIFAR-100-LT		
	$\tau = 0.1$	0.02	0.01	$\tau = 0.1$	0.02	0.01
CE	88.1	76.8	70.2	55.5	41.5	37.4
ETF + DR	88.0	77.8	71.3	54.4	40.6	36.2
NormFace	88.0	79.0	74.3	54.6	40.1	35.9
NTCE	88.8	<b>80.8</b>	<b>77.3</b>	56.8	43.7	39.0
NONL	<b>89.2</b>	80.5	76.3	<b>57.4</b>	<b>44.7</b>	<b>40.0</b>
$\Delta(\text{NONL} - \text{CE})$	+1.2%	+4.8%	+8.7%	+3.4%	+7.7%	+7.0%

497 Table 6: Clean error, mCE, and corruption error (%) on ImageNet-C. Best per column in **green**.  
498

Network	Error	mCE	Noise			Blur			Weather			Digital					
			Gauss	Shot	Impulse	Defoc	Glass	Motion	Zoom	Snow	Frost	Fog	Bright	Contrast	Elastic	Pixel	JPEG
CE	25.0	80.1	75	78	83	<b>84</b>	94	86	88	80	78	68	62	66	96	84	80
ETF + DR	24.6	79.2	75	78	82	86	94	85	86	<b>76</b>	77	66	62	67	93	80	82
NormFace	23.6	77.8	74	76	82	<b>84</b>	<b>93</b>	<b>81</b>	<b>85</b>	<b>76</b>	<b>75</b>	<b>64</b>	<b>60</b>	<b>65</b>	<b>91</b>	81	80
NTCE	<b>23.3</b>	<b>77.6</b>	73	76	<b>80</b>	<b>84</b>	<b>93</b>	83	<b>85</b>	<b>76</b>	<b>75</b>	65	<b>60</b>	<b>65</b>	93	<b>78</b>	<b>79</b>
NONL	23.5	77.8	<b>72</b>	<b>75</b>	<b>80</b>	85	<b>93</b>	83	<b>85</b>	<b>76</b>	<b>75</b>	<b>64</b>	<b>60</b>	66	<b>91</b>	81	81

501  
502  
503  
504  
505  
506 diverse downstream datasets. As shown in Table 4, *NONL consistently yields strong transfer performance*: it attains the best accuracy on 7/8 datasets and delivers a +5.5% relative improvement in mean performance over CE, while NTCE also consistently exceeds CE. These results confirm prior works (Papyan et al., 2020; Bartlett et al., 2017; Neyshabur et al., 2018) that explicitly encouraging NC-like geometry produces features that generalize better beyond the pretraining distribution.

511  
512 **Long-tailed classification.** We next examine robustness to class imbalance using standard eval-  
513 uation pipelines (Yang et al., 2022). For CIFAR-10-LT and CIFAR-100-LT, we construct long-  
514 tailed versions with three imbalance ratios and train all models directly on the imbalanced data.  
515 Table 5 shows that our NC-inducing objectives substantially improve minority-class performance:  
516 on CIFAR-100-LT, NONL outperforms CE by +3.4%, +7.7%, and +7.0% under increasing imbal-  
517 ance, with gains up to +8.7% across CIFAR-10/100-LT, and also surpasses the ETF+DR baseline  
518 (Yang et al., 2022). This suggests that enforcing NC-like geometric structure helps maintain class  
519 separability even when minority classes are severely underrepresented, complementing the improve-  
520 ments observed in transfer.

521  
522 **Out-of-distribution robustness.** Finally, we evaluate robustness to common corruptions on  
523 ImageNet-C (Hendrycks & Dietterich, 2019). Models are trained on clean ImageNet-1K only and  
524 evaluated on corrupted variants, reporting clean top-1 error and mean Corruption Error (mCE) nor-  
525 malized as in Hendrycks & Dietterich (2019). As summarized in Table 6, our normalized losses  
526 reduce mCE compared to CE while also improving clean accuracy. Thus, NC-inducing objectives  
527 not only improve in-distribution performance, but also yield representations that are more robust to  
528 distribution shift, in line with their benefits for transfer and long-tailed recognition.

## 529 6 CONCLUSION

530  
531 In this work, we address the mismatch between the theoretical optima of supervised objectives and  
532 their behavior in practice. Constraining learning to the unit hypersphere removes the radial degen-  
533 eracy of cross-entropy and unifies normalized softmax and supervised contrastive learning (SCL) as  
534 a single prototype-contrast paradigm. Building on this view, we propose two objectives (NTCE and  
535 NONL) that accelerate convergence to Neural Collapse. Theoretically, we prove SCL already yields  
536 an optimal prototype classifier during contrastive training, eliminating the typical linear probing  
537 phase. Empirically, across four benchmarks including ImageNet-1K, our methods surpass CE accu-  
538 racy, reach  $\geq 95\%$  on NC metrics, and attain NC geometry in substantially fewer iterations. Overall,  
539 supervised learning is recast as prototype-based classification on the hypersphere, narrowing the  
theory-practice gap while simplifying and speeding up training.

540 REPRODUCIBILITY STATEMENT  
541

542 Our approach modifies only loss functions within standard pipelines. Results can be replicated by  
543 plugging configurations from Section A.3 into popular codebases (e.g. <https://github.com/HobbitLong/SupContrast>) with minimal effort substituting the original loss with ours.  
544

545  
546 REFERENCES  
547

548 Arthur Albert and John A. Anderson. On the existence of maximum likelihood estimates in logistic  
549 regression models. *Biometrika*, 71(1):1–10, 1984.

550 Peter L. Bartlett, Dylan J. Foster, and Matus Telgarsky. Spectrally-normalized margin bounds for  
551 neural networks. In *Advances in Neural Information Processing Systems (NeurIPS)*, pp. 6241–  
552 6250, 2017.

553 Ting Chen, Simon Kornblith, Mohammad Norouzi, and Geoffrey Hinton. A simple framework for  
554 contrastive learning of visual representations. In *International conference on machine learning*,  
555 pp. 1597–1607. PMLR, 2020.

557 Jiankang Deng, Jia Guo, Niannan Xue, and Stefanos Zafeiriou. Arcface: Additive angular margin  
558 loss for deep face recognition. In *Proceedings of the IEEE/CVF Conference on Computer Vision  
559 and Pattern Recognition (CVPR)*, pp. 4690–4699, 2019.

560 Gavin Weiguang Ding, Yash Sharma, Kry Yik Chau Lui, and Ruitong Huang. Mma training:  
561 Direct input space margin maximization through adversarial training. In *International Conference on  
562 Learning Representations*, 2020. URL <https://openreview.net/forum?id=HkeryxBtPB>.

565 Alhussein Fawzi, Seyed-Mohsen Moosavi-Dezfooli, and Pascal Frossard. Robustness of  
566 classifiers: from adversarial to random noise. In *Advances in Neural Information Pro-  
567 cessing Systems (NeurIPS)*, 2016. URL <https://papers.neurips.cc/paper/6331-robustness-of-classifiers-from-adversarial-to-random-noise.pdf>.

570 Florian Graf, Christoph Hofer, Marc Niethammer, and Roland Kwitt. Dissecting supervised con-  
571 trastive learning. In *International Conference on Machine Learning*, pp. 3821–3830. PMLR,  
572 2021.

573 X.Y. Han, Vardan Papyan, and David L. Donoho. Neural collapse under MSE loss: Proximity to and  
574 dynamics on the central path. In *International Conference on Learning Representations*, 2022.  
575 URL [https://openreview.net/forum?id=w1UbdvWH\\_R3](https://openreview.net/forum?id=w1UbdvWH_R3).

577 Kaiming He, Haoqi Fan, Yuxin Wu, Saining Xie, and Ross Girshick. Momentum contrast for  
578 unsupervised visual representation learning. In *Proceedings of the IEEE/CVF conference on  
579 computer vision and pattern recognition*, pp. 9729–9738, 2020.

580 Matthias Hein and Maksym Andriushchenko. Formal guarantees on the robustness of a classifier  
581 against adversarial manipulation. *Advances in neural information processing systems*, 30, 2017.

583 Dan Hendrycks and Thomas Dietterich. Benchmarking neural network robustness to common cor-  
584 ruptions and perturbations. *Proceedings of the International Conference on Learning Repre-  
585 sentations*, 2019.

586 Yuan Hong and Shuyang Ling. Neural collapse for unconstrained feature model under class-  
587 imbalance. *Journal of Machine Learning Research*, 25(180):1–48, 2024. URL <https://www.jmlr.org/papers/volume25/23-1215/23-1215.pdf>.

590 Prannay Khosla, Piotr Teterwak, Chen Wang, Aaron Sarna, Yonglong Tian, Phillip  
591 Isola, Aaron Maschinot, Ce Liu, and Dilip Krishnan. Supervised contrastive  
592 learning. In *Advances in Neural Information Processing Systems (NeurIPS)*,  
593 2020. URL <https://proceedings.neurips.cc/paper/2020/file/d89a66c7c80a29b1bdbab0f2a1a94af8-Paper.pdf>.

594 Hoyong Kim and Kangil Kim. Fixed non-negative orthogonal classifier: Inducing zero-mean neural  
 595 collapse with feature dimension separation. In *International Conference on Learning Representations (ICLR)*, 2024. URL <https://openreview.net/pdf?id=F4bmOrmUwc>.

596

597

598 Simon Kornblith, Jonathon Shlens, and Quoc V. Le. Do better imagenet models transfer better? In  
 599 *IEEE/CVF Conference on Computer Vision and Pattern Recognition (CVPR)*, pp. 2661–2671,  
 600 2019. URL [https://openaccess.thecvf.com/content\\_CVPR\\_2019/papers/Kornblith\\_Do\\_Better\\_ImageNet\\_Models\\_Transfer\\_Better\\_CVPR\\_2019\\_paper.pdf](https://openaccess.thecvf.com/content_CVPR_2019/papers/Kornblith_Do_Better_ImageNet_Models_Transfer_Better_CVPR_2019_paper.pdf).

601

602

603 Panagiotis Koromilas, Giorgos Bouritsas, Theodoros Giannakopoulos, Mihalis Nicolaou, and Yan-  
 604 nnis Panagakis. Bridging mini-batch and asymptotic analysis in contrastive learning: From infonce  
 605 to kernel-based losses. In *International Conference on Machine Learning*, pp. 25276–25301.  
 606 PMLR, 2024.

607

608 Weiyang Liu, Yandong Wen, Zhiding Yu, Ming Li, Bhiksha Raj, and Le Song. Sphereface: Deep hy-  
 609 persphere embedding for face recognition. In *Proceedings of the IEEE Conference on Computer  
 610 Vision and Pattern Recognition (CVPR)*, pp. 6738–6746, 2017.

611

612 Jianfeng Lu and Stefan Steinerberger. Neural collapse under cross-entropy loss. *Applied and Com-  
 613 putational Harmonic Analysis*, 59:224–241, 2022. doi: 10.1016/j.acha.2021.12.011.

614

615 Evan Markou, Thalaiyasingam Ajanthan, and Stephen Gould. Guiding neural collapse: Optimising  
 616 towards the nearest simplex equiangular tight frame. *Advances in Neural Information Processing  
 Systems*, 37:35544–35573, 2024.

617

618 Aditya Krishna Menon, Sadeep Jayasumana, Ankit Singh Rawat, Himanshu Jain, Andreas Veit, and  
 619 Sanjiv Kumar. Long-tail learning via logit adjustment. In *International Conference on Learning  
 620 Representations*, 2021. URL <https://openreview.net/forum?id=37nvvqkCo5>.

621

622 Pascal Mettes, Elise van der Pol, and Cees G. M. Snoek. Hyperspherical prototype networks. In  
 623 *Advances in Neural Information Processing Systems*, volume 32, 2019.

624

625 Behnam Neyshabur, Srinadh Bhojanapalli, and Nathan Srebro. A pac-bayesian approach to  
 626 spectrally-normalized margin bounds for neural networks. In *International Conference on Learn-  
 627 ing Representations (ICLR)*, 2018. URL [https://openreview.net/forum?id=Skz\\_WfbCZ](https://openreview.net/forum?id=Skz_WfbCZ).

628

629 Vardan Petyan, X. Y. Han, and David L. Donoho. Prevalence of neural collapse during the terminal  
 630 phase of deep learning training. *Proceedings of the National Academy of Sciences*, 117(40):  
 24652–24663, 2020. doi: 10.1073/pnas.2015509117.

631

632 Olivier Roy and Martin Vetterli. The effective rank: A measure of effective dimensionality. In *2007  
 633 15th European signal processing conference*, pp. 606–610. IEEE, 2007.

634

635 Yang Shen, Xuhao Sun, and Xiu-Shen Wei. Equiangular basis vectors. In *Proceedings of the  
 636 IEEE/CVF Conference on Computer Vision and Pattern Recognition*, pp. 16880–16890, 2023.

637

638 Jake Snell, Kevin Swersky, and Richard S. Zemel. Prototypical networks for few-shot learning. In  
 639 *Advances in Neural Information Processing Systems*, volume 30, 2017.

640

641 Kun Song, Zhiqian Tan, Bochao Zou, Huimin Ma, and Weiran Huang. Unveiling the dynamics of  
 642 information interplay in supervised learning. In *International Conference on Machine Learning*,  
 643 pp. 46156–46167. PMLR, 2024.

644

645 Daniel Soudry, Elad Hoffer, Mor Shpigel Nacson, Suriya Gunasekar, and Nathan Srebro. The im-  
 646 plicit bias of gradient descent on separable data. *Journal of Machine Learning Research*, 19(70):  
 647 1–57, 2018. URL <https://jmlr.org/papers/v19/18-188.html>.

648

649 Christos Thrampoulidis, Ganesh Ramachandra Kini, Vala Vakilian, and Tina Behnia. Imbalance  
 650 trouble: Revisiting neural-collapse geometry. *Advances in Neural Information Processing Sys-  
 651 tems*, 35:27225–27238, 2022.

648 Tom Tirer and Joan Bruna. Extended unconstrained features model for exploring deep neural  
 649 collapse. In *Proceedings of the 39th International Conference on Machine Learning*, volume  
 650 162 of *Proceedings of Machine Learning Research*, pp. 21478–21505. PMLR, 2022. URL  
 651 <https://proceedings.mlr.press/v162/tirer22a.html>.

652 Feng Wang, Xiang Xiang, Jian Cheng, and Alan L. Yuille. Normface: L2 hypersphere embedding  
 653 for face verification. In *Proceedings of the 25th ACM International Conference on Multimedia*  
 654 (*MM*), pp. 1041–1049, 2017. doi: 10.1145/3123266.3123359.

655 Hao Wang, Yitong Wang, Zheng Zhou, Xing Ji, Dihong Gong, Jingchao Zhou, Zhifeng Li, and  
 656 Wei Liu. Cosface: Large margin cosine loss for deep face recognition. In *Proceedings of the*  
 657 *IEEE/CVF Conference on Computer Vision and Pattern Recognition (CVPR)*, pp. 5265–5274,  
 658 2018.

659 Tongzhou Wang and Phillip Isola. Understanding contrastive representation learning through align-  
 660 ment and uniformity on the hypersphere. In *International conference on machine learning*, pp.  
 661 9929–9939. PMLR, 2020.

662 Xudong Wang, Ziwei Liu, and Stella X Yu. Unsupervised feature learning by cross-level instance-  
 663 group discrimination. In *Proceedings of the IEEE/CVF conference on computer vision and pattern*  
 664 *recognition*, pp. 12586–12595, 2021.

665 Yibo Yang, Shixiang Chen, Xiangtai Li, Liang Xie, Zhouchen Lin, and Dacheng Tao. Inducing  
 666 neural collapse in imbalanced learning: Do we really need a learnable classifier at the end of  
 667 deep neural network? In *Advances in Neural Information Processing Systems*, volume 35, pp.  
 668 37991–38002, 2022.

669 Can Yaras, Peng Wang, Zhihui Zhu, Laura Balzano, and Qing Qu. Neural collapse with normalized  
 670 features: A geometric analysis over the riemannian manifold. In *Advances in Neural Information*  
 671 *Processing Systems (NeurIPS)*, 2022.

672 Chun-Hsiao Yeh, Cheng-Yao Hong, Yen-Chi Hsu, Tyng-Luh Liu, Yubei Chen, and Yann LeCun.  
 673 Decoupled contrastive learning. In *European Conference on Computer Vision*, pp. 668–684.  
 674 Springer, 2022.

675 Shuoxi Zhang, Zijian Song, and Kun He. Neural collapse inspired knowledge distillation. In *Pro-  
 676 ceedings of the AAAI Conference on Artificial Intelligence*, volume 39, pp. 22542–22550, 2025.

677 Yifan Zhang, Zhiqian Tan, Jingqin Yang, Weiran Huang, and Yang Yuan. Matrix information theory  
 678 for self-supervised learning. In *Proceedings of the 41st International Conference on Machine*  
 679 *Learning*, pp. 59897–59918, 2024.

680 Jinxin Zhou, Xiao Li, Tianyu Ding, Chong You, Qing Qu, and Zhihui Zhu. On the optimization  
 681 landscape of neural collapse under mse loss: Global optimality with unconstrained features. In  
 682 *International Conference on Machine Learning*, pp. 27179–27202. PMLR, 2022a.

683 Jinxin Zhou, Chong You, Xiao Li, Kangning Liu, Sheng Liu, Qing Qu, and Zhi-  
 684 hui Zhu. Are all losses created equal: A neural collapse perspective. In  
 685 *Advances in Neural Information Processing Systems (NeurIPS)*, 2022b. URL  
 686 [https://proceedings.neurips.cc/paper\\_files/paper/2022/file/cdce17de141c9fba3bdf175a0b721941-Paper-Conference.pdf](https://proceedings.neurips.cc/paper_files/paper/2022/file/cdce17de141c9fba3bdf175a0b721941-Paper-Conference.pdf).

687 Zhihui Zhu, Tianyu Ding, Jinxin Zhou, Xiao Li, Chong You, Jeremias Sulam, and Qing Qu. A ge-  
 688 ometric analysis of neural collapse with unconstrained features. *Advances in Neural Information*  
 689 *Processing Systems*, 34:29820–29834, 2021.

690

691

692

693

694

695

696

697 **A APPENDIX**

698

699 **A.1 NEURAL COLLAPSE OPTIMALITY OF NORMALIZED OBJECTIVES**

700

701 We adopt the balanced unconstrained-features / layer-peeled model (UFM/LPM) (Tirer & Bruna,  
 702 2022; Yaras et al., 2022). The last-layer features  $z_i \in \mathbb{R}^d$  and classifier weights  $w_c \in \mathbb{R}^d$  are free

702 optimization variables. We work with their  $\ell_2$ -normalized versions  
 703

$$704 \quad \mathbf{u}_i = \frac{\mathbf{z}_i}{\|\mathbf{z}_i\|}, \quad \hat{\mathbf{w}}_c = \frac{\mathbf{w}_c}{\|\mathbf{w}_c\|},$$

705 so that  $\|\mathbf{u}_i\| = \|\hat{\mathbf{w}}_c\| = 1$  and  
 706

$$707 \quad S_{ic} := \mathbf{u}_i^\top \hat{\mathbf{w}}_c.$$

708 There are  $K$  classes and  $M$  training samples, and the dataset is balanced: each class  $c$  has index set  
 709

$$709 \quad I_c := \{i : y_i = c\} \quad \text{with} \quad |I_c| = n = M/K.$$

710 We assume  $d \geq K$ .  
 711

712 **Normalized CE-based losses.** We consider three normalized cross-entropy-based losses with  
 713 temperature  $\tau > 0$ :

$$714 \quad \mathcal{L}_{\text{NF}} = -\frac{1}{M} \sum_{i=1}^M \log \frac{\exp(S_{i,y_i}/\tau)}{\sum_{c=1}^K \exp(S_{ic}/\tau)}, \quad (8)$$

$$715 \quad \mathcal{L}_{\text{NTCE}} = -\frac{1}{M} \sum_{i=1}^M \log \frac{\exp(S_{i,y_i}/\tau)}{\sum_{j=1}^M \exp(S_{j,y_i}/\tau)}, \quad (9)$$

$$716 \quad \mathcal{L}_{\text{NONL}} = -\frac{1}{M} \sum_{i=1}^M \log \frac{\exp(S_{i,y_i}/\tau)}{\sum_{j: y_j \neq y_i} \exp(S_{j,y_i}/\tau)}. \quad (10)$$

717 **Neural Collapse properties.** We say a configuration exhibits *Neural Collapse* (NC) if there exist  
 718 unit vectors  $\mu_1, \dots, \mu_K \in \mathbb{R}^d$  such that:  
 719

720 (NC1) (Within-class collapse)  $\mathbf{u}_i = \mu_{y_i}$  for all  $i$ .  
 721

722 (NC2) (Simplex ETF) the vectors  $\{\mu_c\}$  form a centered regular simplex in a  $(K-1)$ -dimensional sub-  
 723 space:  
 724

$$725 \quad \|\mu_c\| = 1 \quad \text{and} \quad \mu_c^\top \mu_{c'} = -\frac{1}{K-1} \quad \forall c \neq c'.$$

726 (NC3) (Classifier-mean alignment)  $\hat{\mathbf{w}}_c = \mu_c$  for all  $c$ .  
 727

728 At such a configuration the (normalized-feature) class means  $\hat{\mu}_c := \frac{1}{n} \sum_{i \in I_c} \mathbf{u}_i$  coincide with  $\mu_c$   
 729 and are therefore unit norm.  
 730

731 **Theorem A.1** (NC optimality of normalized CE-based losses). *In the balanced UFM/LPM setting  
 732 above with  $d \geq K$ , every global minimizer of  $\mathcal{L}_{\text{NF}}$ ,  $\mathcal{L}_{\text{NTCE}}$ , and  $\mathcal{L}_{\text{NONL}}$  satisfies NC1–NC3, up to  
 733 a global rotation and permutation of class labels.*

734 We now analyze the three losses in turn.  
 735

## 736 NORMFACE

737 Yaras et al. (2022) study the constrained UFM problem  
 738

$$739 \quad \min_{H, W} \frac{1}{M} \sum_{i=1}^M \text{CE}(\tau' W^\top \mathbf{h}_i, y_i) \quad \text{s.t. } \|\mathbf{h}_i\| = 1, \|\mathbf{w}_c\| = 1, \quad (11)$$

740 with  $\tau' > 0$ , where CE is the standard cross-entropy.  
 741

742 **Lemma A.2** (NormFace  $\equiv$  Yaras et al.). *Set  $\tau' = 1/\tau$ , and identify  $\mathbf{h}_i = \mathbf{u}_i$  and  $\mathbf{w}_c = \hat{\mathbf{w}}_c$ . Then  
 743  $\mathcal{L}_{\text{NF}}$  coincides with equation 11, and  $\arg \min \mathcal{L}_{\text{NF}}$  equals the set of global minimizers of equation 11  
 744 over unit-norm features and weights.*

745 *Proof.* With  $\mathbf{h}_i = \mathbf{u}_i$ ,  $\mathbf{w}_c = \hat{\mathbf{w}}_c$  and  $\tau' = 1/\tau$ , we have  $(\tau' W^\top \mathbf{h}_i)_c = S_{ic}/\tau$ , so the summand  
 746 in equation 11 is exactly  $-\log \frac{\exp(S_{i,y_i}/\tau)}{\sum_c \exp(S_{ic}/\tau)}$ , which is the  $i$ th summand in  $\mathcal{L}_{\text{NF}}$ . Averaging over  $i$   
 747 gives the claim.  $\square$   
 748

749 Theorem 3.1 of Yaras et al. (2022) states that, under balanced labels and  $d \geq K$ , every global  
 750 minimizer of equation 11 satisfies NC1–NC3. Together with Lemma A.2, this implies that every  
 751 global minimizer of  $\mathcal{L}_{\text{NF}}$  satisfies NC1–NC3.  
 752

756 NTCE

757

758 We now show that every global minimizer of  $\mathcal{L}_{\text{NTCE}}$  satisfies NC1–NC3. The proof follows the  
 759 same three-step pattern we later use for NONL: we first reduce to a class-level objective depending  
 760 only on class means and weights, then view this function as a contrastive loss of La/Lc type from  
 761 (Koromilas et al., 2024) and apply its respective minimizer characterization at the class level, and  
 762 finally lift the resulting structure back to the sample level.

763 Recall that

$$764 \mathcal{L}_{\text{NTCE}} = -\frac{1}{M} \sum_{i=1}^M \log \frac{\exp(\mathbf{u}_i^\top \hat{\mathbf{w}}_{y_i}/\tau)}{\sum_{j=1}^M \exp(\mathbf{u}_j^\top \hat{\mathbf{w}}_{y_i}/\tau)} = \frac{1}{M} \sum_{i=1}^M \ell_i^{\text{NTCE}},$$

765 with per-sample loss

$$766 \ell_i^{\text{NTCE}} := -\log \frac{\exp(\mathbf{u}_i^\top \hat{\mathbf{w}}_{y_i}/\tau)}{\sum_{j=1}^M \exp(\mathbf{u}_j^\top \hat{\mathbf{w}}_{y_i}/\tau)}.$$

767 We again work in the balanced setting  $|I_c| = n = M/K$  and  $\|\mathbf{u}_i\| = \|\hat{\mathbf{w}}_c\| = 1$ .

768 **Step 1: reduction to class means.**

769 **Lemma A.3** (NTCE reduction via class means). *Assume balanced labels,  $|I_c| = n = M/K$  for all  
 770  $c$ . For any configuration  $\{\mathbf{u}_i\}, \{\hat{\mathbf{w}}_c\}$  with  $\|\mathbf{u}_i\| = \|\hat{\mathbf{w}}_c\| = 1$  define the normalized-feature class  
 771 means*

$$772 \hat{\boldsymbol{\mu}}_c := \frac{1}{n} \sum_{j \in I_c} \mathbf{u}_j.$$

773 Then

$$774 \mathcal{L}_{\text{NTCE}}(\{\mathbf{u}_i\}, \{\hat{\mathbf{w}}_c\}) \geq L_{\text{NTCE}}^{\text{cls}}(\{\hat{\boldsymbol{\mu}}_c\}, \{\hat{\mathbf{w}}_c\}),$$

775 where the class-level loss is

$$776 L_{\text{NTCE}}^{\text{cls}} := -\frac{1}{K\tau} \sum_{c=1}^K \hat{\mathbf{w}}_c^\top \hat{\boldsymbol{\mu}}_c + \frac{1}{K} \sum_{c=1}^K \log \left( \sum_{c'=1}^K n \exp(\hat{\mathbf{w}}_c^\top \hat{\boldsymbol{\mu}}_{c'}/\tau) \right). \quad (12)$$

777 Moreover, the inequality is tight if and only if, for every ordered pair  $(c, c')$ , the logits  $\hat{\mathbf{w}}_c^\top \mathbf{u}_j$  are  
 778 constant over  $j \in I_{c'}$ , i.e.

$$779 \hat{\mathbf{w}}_c^\top \mathbf{u}_j = \hat{\mathbf{w}}_c^\top \hat{\boldsymbol{\mu}}_{c'} \quad \text{for all } j \in I_{c'}.$$

780 *Proof.* Fix a configuration  $\{\mathbf{u}_i\}, \{\hat{\mathbf{w}}_c\}$  and define the class means  $\hat{\boldsymbol{\mu}}_c$  as above. Using the balanced  
 781 labels, write  $\mathcal{L}_{\text{NTCE}}$  as an average over classes. For  $i \in I_c$  we have

$$782 \ell_i^{\text{NTCE}} = -\frac{1}{\tau} \hat{\mathbf{w}}_c^\top \mathbf{u}_i + \log \left( \sum_{j=1}^M \exp(\hat{\mathbf{w}}_c^\top \mathbf{u}_j/\tau) \right),$$

783 so

$$784 \mathcal{L}_{\text{NTCE}} = \frac{1}{M} \sum_{c=1}^K \sum_{i \in I_c} \ell_i^{\text{NTCE}} \\ 785 = -\frac{1}{M\tau} \sum_{c=1}^K \sum_{i \in I_c} \hat{\mathbf{w}}_c^\top \mathbf{u}_i + \frac{1}{M} \sum_{c=1}^K \sum_{i \in I_c} \log \left( \sum_{j=1}^M \exp(\hat{\mathbf{w}}_c^\top \mathbf{u}_j/\tau) \right).$$

802 The denominator term inside the logarithm depends only on the anchor class  $c$ , not on  $i$ , so  $\sum_{i \in I_c}$   
 803 introduces a factor of  $|I_c| = n$ . Using  $M = nK$  and the definition of  $\hat{\boldsymbol{\mu}}_c$  we obtain

$$804 \mathcal{L}_{\text{NTCE}} = -\frac{1}{K\tau} \sum_{c=1}^K \hat{\mathbf{w}}_c^\top \left( \frac{1}{n} \sum_{i \in I_c} \mathbf{u}_i \right) + \frac{1}{K} \sum_{c=1}^K \log \left( \sum_{j=1}^M \exp(\hat{\mathbf{w}}_c^\top \mathbf{u}_j/\tau) \right) \\ 805 = -\frac{1}{K\tau} \sum_{c=1}^K \hat{\mathbf{w}}_c^\top \hat{\boldsymbol{\mu}}_c + \frac{1}{K} \sum_{c=1}^K \log \left( \sum_{j=1}^M \exp(\hat{\mathbf{w}}_c^\top \mathbf{u}_j/\tau) \right).$$

810 For each fixed anchor class  $c$ , split the denominator over classes:  
 811

$$812 \quad \sum_{j=1}^M \exp(\hat{\mathbf{w}}_c^\top \mathbf{u}_j / \tau) = \sum_{c'=1}^K \sum_{j \in I_{c'}} \exp(\hat{\mathbf{w}}_c^\top \mathbf{u}_j / \tau).$$

$$813$$

$$814$$

815 For fixed  $(c, c')$ , the function  $f_c(\mathbf{x}) := \exp(\hat{\mathbf{w}}_c^\top \mathbf{x} / \tau)$  is convex in  $\mathbf{x}$ , so by Jensen's inequality over  
 816  $j \in I_{c'}$ ,  
 817

$$818 \quad \frac{1}{n} \sum_{j \in I_{c'}} \exp(\hat{\mathbf{w}}_c^\top \mathbf{u}_j / \tau) = \frac{1}{n} \sum_{j \in I_{c'}} f_c(\mathbf{u}_j) \geq f_c\left(\frac{1}{n} \sum_{j \in I_{c'}} \mathbf{u}_j\right) = \exp(\hat{\mathbf{w}}_c^\top \hat{\boldsymbol{\mu}}_{c'} / \tau).$$

$$819$$

$$820$$

821 Multiplying by  $n$  and summing over  $c'$  yields

$$822 \quad \sum_{j=1}^M \exp(\hat{\mathbf{w}}_c^\top \mathbf{u}_j / \tau) \geq \sum_{c'=1}^K n \exp(\hat{\mathbf{w}}_c^\top \hat{\boldsymbol{\mu}}_{c'} / \tau).$$

$$823$$

$$824$$

825 Taking logs and averaging over  $c$  gives  
 826

$$827 \quad \mathcal{L}_{\text{NTCE}} \geq -\frac{1}{K\tau} \sum_{c=1}^K \hat{\mathbf{w}}_c^\top \hat{\boldsymbol{\mu}}_c + \frac{1}{K} \sum_{c=1}^K \log \left( \sum_{c'=1}^K n \exp(\hat{\mathbf{w}}_c^\top \hat{\boldsymbol{\mu}}_{c'} / \tau) \right) = L_{\text{NTCE}}^{\text{cls}}.$$

$$828$$

$$829$$

830 Jensen's inequality is tight for a given pair  $(c, c')$  if and only if the arguments of  $f_c$  are constant over  
 831  $j \in I_{c'}$ , i.e. if and only if  $\hat{\mathbf{w}}_c^\top \mathbf{u}_j$  is constant in  $j$  on  $I_{c'}$ . In that case this constant must equal  $\hat{\mathbf{w}}_c^\top \hat{\boldsymbol{\mu}}_{c'}$ .  
 832 Tightness for all  $c, c'$  gives the stated condition.  $\square$   
 833

834 Thus, for any configuration of unit features and weights, the NTCE loss is lower-bounded by the  
 835 class-level objective  $L_{\text{NTCE}}^{\text{cls}}$  depending only on the  $K$  class means  $\hat{\boldsymbol{\mu}}_c$  and the  $K$  classifier weights  
 836  $\hat{\mathbf{w}}_c$ , and Lemma A.3 precisely characterizes when this lower bound is tight (blockwise constant  
 837 logits).  
 838

839 It is convenient to separate out the constant  $\log n$  factor, and to view the class means and weights  
 840 abstractly as unit vectors. Define the *normalized* class-level NTCE loss

$$841 \quad \tilde{L}_{\text{NTCE}}^{\text{cls}}(\{\hat{\boldsymbol{\mu}}_c\}, \{\hat{\mathbf{w}}_c\}) := -\frac{1}{K\tau} \sum_{c=1}^K \hat{\mathbf{w}}_c^\top \hat{\boldsymbol{\mu}}_c + \frac{1}{K} \sum_{c=1}^K \log \left( \sum_{c'=1}^K \exp(\hat{\mathbf{w}}_c^\top \hat{\boldsymbol{\mu}}_{c'} / \tau) \right),$$

$$842$$

$$843$$

844 so that

$$845 \quad L_{\text{NTCE}}^{\text{cls}} = \log n + \tilde{L}_{\text{NTCE}}^{\text{cls}}.$$

$$846$$

847 In what follows, we treat the pairs  $(\hat{\boldsymbol{\mu}}_c, \hat{\mathbf{w}}_c)$  as free variables on the unit sphere and, to lighten  
 848 notation, write  $\boldsymbol{\mu}_c := \hat{\boldsymbol{\mu}}_c$  and  $\mathbf{w}_c := \hat{\mathbf{w}}_c$ .  
 849

850 **Step 2: analysis of the class-level problem.** For each class  $c$  we view the  $c$ th summand in  $\tilde{L}_{\text{NTCE}}^{\text{cls}}$   
 851 as a standard contrastive loss of La/Lc type (Koromilas et al., 2024), with

$$852 \quad q_c = \mathbf{w}_c \quad (\text{anchor}), \quad k_c^+ = \boldsymbol{\mu}_c \quad (\text{positive}), \quad \{k_c^- = \boldsymbol{\mu}_{c'} : c' \neq c\} \quad (\text{negatives}).$$

$$853$$

854 The per-class alignment and contrastive terms are  
 855

$$856 \quad L_a(q_c, k_c^+) = -\frac{1}{\tau} q_c^\top k_c^+, \quad L_c(q_c, \{k_c^-\}) = \log \left( \sum_{c'=1}^K \exp(q_c^\top k_c^- / \tau) \right).$$

$$857$$

$$858$$

859 The La/Lc framework requires  $L_a$  to be strictly decreasing in similarity and  $L_c$  to be convex and  
 860 strictly increasing in similarity. These conditions hold here:

861 •  $q_c^\top k_c^+$  enters  $L_a$  linearly with a negative coefficient, so  $L_a$  decreases as  $q_c^\top k_c^+$  increases.  
 862 •  $L_c$  is a log-sum-exp of the similarities  $q_c^\top k_c^- / \tau$ , hence convex and strictly increasing in each  
 863 similarity argument.

864 Therefore we may invoke the minimizer characterization for La/Lc losses. By Theorem 4.1 and  
 865 Appendix B.1 of Koromilas et al. (2024), provided  $d \geq K$ , the global minimizers of  $\tilde{L}_{\text{NTCE}}^{\text{cls}}$  over  
 866 unit vectors satisfy:

867

- 868 • **Perfect alignment:**  $\mu_c = w_c$  for all  $c$ .
- 869 • **Simplex ETF structure:** the directions  $\{\mu_c\}_{c=1}^K$  form a centered regular simplex equiangular  
 870 tight frame in a  $(K-1)$ -dimensional subspace:

871

$$872 \|\mu_c\| = 1, \quad \mu_c^\top \mu_{c'} = -\frac{1}{K-1} \quad \forall c \neq c'.$$

873

874 In particular, there exists a simplex ETF  $\{\mu_c\}_{c=1}^K \subset \mathbb{R}^d$  such that  $\mu_c = w_c$  is a global minimizer of  
 875  $\tilde{L}_{\text{NTCE}}^{\text{cls}}$ , unique up to a global rotation and permutation of the class indices.

876

877 **Step 3: lifting back to the sample level.** We now relate these class-level minimizers back to the  
 878 original sample-level NTCE objective and derive the NC structure of its global minimizers.

879

880 *Existence of Neural Collapse minimizers.* Let  $\{\mu_c\}_{c=1}^K$  be a simplex ETF and set

881

$$\hat{w}_c := \mu_c, \quad u_i := \mu_{y_i} \quad \text{for all } i.$$

882

883 This configuration satisfies NC1–NC3 by construction: within each class  $c$ , all normalized features  
 884 collapse to  $\mu_c$  (NC1), the vectors  $\{\mu_c\}$  form a centered simplex ETF (NC2), and  $\hat{w}_c = \mu_c$  (NC3).  
 885 In particular, the feature class means are  $\hat{\mu}_c = \mu_c$ .

886 Moreover, for this configuration the Jensen inequalities in Lemma A.3 are tight: for any anchor class  
 887  $c$  and any class  $c'$ , we have  $\hat{w}_c^\top u_j = \mu_c^\top \mu_{c'}$  for all  $j \in I_{c'}$ , so the logits are constant within each  
 888 class. Hence

889

$$890 \mathcal{L}_{\text{NTCE}} = L_{\text{NTCE}}^{\text{cls}}(\{\hat{\mu}_c\}, \{\hat{w}_c\}) = \log n + \tilde{L}_{\text{NTCE}}^{\text{cls}}(\{\mu_c\}, \{\mu_c\}).$$

891 Since  $\{\mu_c\}, \{\mu_c\}$  is a global minimizer of  $\tilde{L}_{\text{NTCE}}^{\text{cls}}$ , this shows that

892

$$893 \inf_{\{u_i\}, \{\hat{w}_c\}} \mathcal{L}_{\text{NTCE}} \leq \log n + \inf_{\{\mu_c\}, \{w_c\}} \tilde{L}_{\text{NTCE}}^{\text{cls}}.$$

894

895 *Structure of arbitrary global minimizers.* Conversely, let  $(\{u_i^*\}, \{\hat{w}_c^*\})$  be any global minimizer of  
 896  $\mathcal{L}_{\text{NTCE}}$ , and let

897

$$898 \hat{\mu}_c^* := \frac{1}{n} \sum_{j \in I_c} u_j^*$$

899

900 be the corresponding class means. Lemma A.3 gives

901

$$902 \mathcal{L}_{\text{NTCE}}(\{u_i^*\}, \{\hat{w}_c^*\}) \geq L_{\text{NTCE}}^{\text{cls}}(\{\hat{\mu}_c^*\}, \{\hat{w}_c^*\}) = \log n + \tilde{L}_{\text{NTCE}}^{\text{cls}}(\{\hat{\mu}_c^*\}, \{\hat{w}_c^*\}).$$

903 On the other hand, from the ETF construction above we know that

904

$$905 \inf_{\{u_i\}, \{\hat{w}_c\}} \mathcal{L}_{\text{NTCE}} \leq \log n + \inf_{\{\mu_c\}, \{w_c\}} \tilde{L}_{\text{NTCE}}^{\text{cls}}.$$

906

907 Since  $(\{u_i^*\}, \{\hat{w}_c^*\})$  achieves the global infimum, the two displays must be equalities. Therefore:

908 •  $\tilde{L}_{\text{NTCE}}^{\text{cls}}(\{\hat{\mu}_c^*\}, \{\hat{w}_c^*\})$  attains the global minimum of  $\tilde{L}_{\text{NTCE}}^{\text{cls}}$ , so by the La/Lc minimizer charac-  
 909 terization we must have, up to a global rotation and permutation of class labels,

910

$$911 \hat{\mu}_c^* = \hat{w}_c^* \quad \text{for all } c, \quad \{\hat{\mu}_c^*\} \text{ form a centered simplex ETF.}$$

912

- 913 • Lemma A.3 must be tight at the minimizer, so the Jensen equalities hold for all  $(c, c')$ : for every  
 914 anchor class  $c$  and every class  $c'$ , the logits  $\hat{w}_c^{*\top} u_j^*$  are constant over  $j \in I_{c'}$ , equal to  $\hat{w}_c^{*\top} \hat{\mu}_{c'}^*$ .

915 Let  $S := \text{span}\{\hat{w}_1^*, \dots, \hat{w}_K^*\}$ , which is the  $(K-1)$ -dimensional simplex-ETF subspace. Fix a  
 916 class  $c'$  and  $j \in I_{c'}$ . For every  $c \neq c'$ , tightness of Jensen gives

917

$$\hat{w}_c^{*\top} (u_j^* - \hat{\mu}_{c'}^*) = 0.$$

918 Since  $\{\hat{\mathbf{w}}_c^*\}_{c=1}^K$  form a centered simplex ETF in the  $(K - 1)$ -dimensional subspace  $S$  and satisfy  
 919  $\sum_{c=1}^K \hat{\mathbf{w}}_c^* = 0$ , any  $K - 1$  of them are linearly independent and thus span  $S$ . In particular, the set  
 920  $\{\hat{\mathbf{w}}_c^* : c \neq c'\}$  spans  $S$ , so  $\mathbf{u}_j^* - \hat{\boldsymbol{\mu}}_{c'}^*$  is orthogonal to  $S$ , and hence the orthogonal projection of  $\mathbf{u}_j^*$   
 921 onto  $S$  equals  $\hat{\boldsymbol{\mu}}_{c'}^*$ .  
 922

923 But both  $\mathbf{u}_j^*$  and  $\hat{\boldsymbol{\mu}}_{c'}^* = \hat{\mathbf{w}}_{c'}^*$  are unit vectors, and  $\hat{\boldsymbol{\mu}}_{c'}^* \in S$ . The only way for a unit vector to have a  
 924 unit-norm projection onto  $S$  is to lie in  $S$  itself and coincide with its projection, so we must have

$$925 \quad \mathbf{u}_j^* = \hat{\boldsymbol{\mu}}_{c'}^* \quad \text{for all } j \in I_{c'}.$$

927 Thus within each class all features collapse to a single unit direction (NC1), these  $K$  directions  
 928 form a centered simplex ETF (NC2), and the classifier weights align with the class means (NC3).  
 929 Therefore every global minimizer of  $\mathcal{L}_{\text{NTCE}}$  exhibits Neural Collapse, up to a global rotation and  
 930 permutation of the class labels.

### 931 NONL

933 We finally treat the NONL objective equation 10. The proof proceeds by first bounding the sample-  
 934 level loss by a class-level objective depending only on class means and weights, then applying the  
 935 La/Lc minimizer characterization at the class level, and finally lifting this structure back to the  
 936 sample level to obtain NC1–NC3.

937 Recall that

$$939 \quad \mathcal{L}_{\text{NONL}} = -\frac{1}{M} \sum_{i=1}^M \log \frac{\exp(S_{i,y_i}/\tau)}{\sum_{j: y_j \neq y_i} \exp(S_{j,y_i}/\tau)} = \frac{1}{M} \sum_{i=1}^M \ell_i^{\text{NONL}},$$

942 with per-sample loss

$$943 \quad \ell_i^{\text{NONL}} := -\log \frac{\exp(\mathbf{u}_i^\top \hat{\mathbf{w}}_{y_i}/\tau)}{\sum_{j: y_j \neq y_i} \exp(\mathbf{u}_j^\top \hat{\mathbf{w}}_{y_i}/\tau)}.$$

945 We again work in the balanced setting  $|I_c| = n = M/K$  and  $\|\mathbf{u}_i\| = \|\hat{\mathbf{w}}_c\| = 1$ .

947 **Step 1: reduction to class means.** We first show that the sample-level NONL loss admits a lower  
 948 bound that depends only on the  $K$  normalized-feature class means and the  $K$  classifier weights.

949 **Lemma A.4** (NONL reduction via class means). *Assume balanced labels,  $|I_c| = n = M/K$  for all  
 950  $c$ . For any configuration  $\{\mathbf{u}_i\}, \{\hat{\mathbf{w}}_c\}$  with  $\|\mathbf{u}_i\| = \|\hat{\mathbf{w}}_c\| = 1$  define the normalized-feature class  
 951 means*

$$952 \quad \hat{\boldsymbol{\mu}}_c := \frac{1}{n} \sum_{j \in I_c} \mathbf{u}_j.$$

954 Then

$$955 \quad \mathcal{L}_{\text{NONL}}(\{\mathbf{u}_i\}, \{\hat{\mathbf{w}}_c\}) \geq L_{\text{NONL}}^{\text{cls}}(\{\hat{\boldsymbol{\mu}}_c\}, \{\hat{\mathbf{w}}_c\}),$$

956 where the class-level loss is

$$958 \quad L_{\text{NONL}}^{\text{cls}} := -\frac{1}{K\tau} \sum_{c=1}^K \hat{\mathbf{w}}_c^\top \hat{\boldsymbol{\mu}}_c + \frac{1}{K} \sum_{c=1}^K \log \left( \sum_{c' \neq c} n \exp(\hat{\mathbf{w}}_c^\top \hat{\boldsymbol{\mu}}_{c'}/\tau) \right). \quad (13)$$

961 Moreover, the inequality is tight if and only if, for every ordered pair  $(c, c')$  with  $c' \neq c$ , the “negative”  
 962 logits  $\hat{\mathbf{w}}_c^\top \mathbf{u}_j$  are constant over  $j \in I_{c'}$ , i.e.

$$963 \quad \hat{\mathbf{w}}_c^\top \mathbf{u}_j = \hat{\mathbf{w}}_c^\top \hat{\boldsymbol{\mu}}_{c'} \quad \text{for all } j \in I_{c'}, c' \neq c.$$

965 *Proof.* Fix a sample index  $i$  with label  $y_i = c$ . Its NONL denominator is

$$967 \quad D_i^{\text{neg}} := \sum_{j: y_j \neq c} \exp(\mathbf{u}_j^\top \hat{\mathbf{w}}_c/\tau) = \sum_{c' \neq c} \sum_{j \in I_{c'}} \exp(\mathbf{u}_j^\top \hat{\mathbf{w}}_c/\tau).$$

970 For each anchor class  $c$  and negative class  $c' \neq c$ , consider the function

$$971 \quad f_c(\mathbf{x}) := \exp(\hat{\mathbf{w}}_c^\top \mathbf{x}/\tau),$$

972 which is convex in  $\mathbf{x}$ . Applying Jensen's inequality over the negative-class samples  $\{\mathbf{u}_j : j \in I_{c'}\}$   
 973 gives  
 974

$$975 \frac{1}{n} \sum_{j \in I_{c'}} \exp(\hat{\mathbf{w}}_c^\top \mathbf{u}_j / \tau) = \frac{1}{n} \sum_{j \in I_{c'}} f_c(\mathbf{u}_j) \geq f_c\left(\frac{1}{n} \sum_{j \in I_{c'}} \mathbf{u}_j\right) = \exp(\hat{\mathbf{w}}_c^\top \hat{\boldsymbol{\mu}}_{c'} / \tau).$$

978 Multiplying by  $n$  and summing over  $c' \neq c$  yields  
 979

$$980 D_i^{\text{neg}} = \sum_{c' \neq c} \sum_{j \in I_{c'}} \exp(\mathbf{u}_j^\top \hat{\mathbf{w}}_c / \tau) \geq \sum_{c' \neq c} n \exp(\hat{\mathbf{w}}_c^\top \hat{\boldsymbol{\mu}}_{c'} / \tau).$$

982 By definition of  $\ell_i^{\text{NONL}}$ ,  
 983

$$984 \ell_i^{\text{NONL}} = -\log \frac{\exp(\mathbf{u}_i^\top \hat{\mathbf{w}}_c / \tau)}{D_i^{\text{neg}}}$$

$$985 = -\frac{1}{\tau} \hat{\mathbf{w}}_c^\top \mathbf{u}_i + \log D_i^{\text{neg}}$$

$$986 \geq -\frac{1}{\tau} \hat{\mathbf{w}}_c^\top \mathbf{u}_i + \log \left( \sum_{c' \neq c} n \exp(\hat{\mathbf{w}}_c^\top \hat{\boldsymbol{\mu}}_{c'} / \tau) \right) =: \tilde{\ell}_i.$$

992 This inequality is tight if and only if all Jensen steps above are equalities. For a fixed  $(c, c')$  with  
 993  $c' \neq c$ , equality in Jensen requires that the arguments of  $f_c$  be constant over  $j \in I_{c'}$ , i.e.  $\hat{\mathbf{w}}_c^\top \mathbf{u}_j$  is  
 994 constant on  $I_{c'}$ . Using the definition of  $\hat{\boldsymbol{\mu}}_{c'}$ , this constant must then equal  $\hat{\mathbf{w}}_c^\top \hat{\boldsymbol{\mu}}_{c'}$ , giving the stated  
 995 tightness condition.

996 Finally, average  $\tilde{\ell}_i$  over all samples. Using the balanced labels  $|I_c| = n$  and the definition of  $\hat{\boldsymbol{\mu}}_c$ ,  
 997

$$998 \frac{1}{M} \sum_{i=1}^M \tilde{\ell}_i = \frac{1}{M} \sum_{c=1}^K \sum_{i \in I_c} \left[ -\frac{1}{\tau} \hat{\mathbf{w}}_c^\top \mathbf{u}_i + \log \left( \sum_{c' \neq c} n \exp(\hat{\mathbf{w}}_c^\top \hat{\boldsymbol{\mu}}_{c'} / \tau) \right) \right]$$

$$1000 = -\frac{1}{M\tau} \sum_{c=1}^K \sum_{i \in I_c} \hat{\mathbf{w}}_c^\top \mathbf{u}_i + \frac{1}{M} \sum_{c=1}^K |I_c| \log \left( \sum_{c' \neq c} n \exp(\hat{\mathbf{w}}_c^\top \hat{\boldsymbol{\mu}}_{c'} / \tau) \right)$$

$$1002 = -\frac{1}{K\tau} \sum_{c=1}^K \hat{\mathbf{w}}_c^\top \hat{\boldsymbol{\mu}}_c + \frac{1}{K} \sum_{c=1}^K \log \left( \sum_{c' \neq c} n \exp(\hat{\mathbf{w}}_c^\top \hat{\boldsymbol{\mu}}_{c'} / \tau) \right)$$

$$1004 = L_{\text{NONL}}^{\text{cls}}(\{\hat{\boldsymbol{\mu}}_c\}, \{\hat{\mathbf{w}}_c\}).$$

1009 Since  $\mathcal{L}_{\text{NONL}}$  is the average of the  $\ell_i^{\text{NONL}}$  and each  $\ell_i^{\text{NONL}} \geq \tilde{\ell}_i$ , we obtain  $\mathcal{L}_{\text{NONL}} \geq L_{\text{NONL}}^{\text{cls}}$  with  
 1010 the stated equality condition.  $\square$

1012 As before, it is convenient to separate out the factor  $n$  from the logarithm and to treat the class means  
 1013 and weights abstractly as unit vectors. Define the *normalized* class-level NONL loss  
 1014

$$1015 \tilde{L}_{\text{NONL}}^{\text{cls}}(\{\hat{\boldsymbol{\mu}}_c\}, \{\hat{\mathbf{w}}_c\}) := -\frac{1}{K\tau} \sum_{c=1}^K \hat{\mathbf{w}}_c^\top \hat{\boldsymbol{\mu}}_c + \frac{1}{K} \sum_{c=1}^K \log \left( \sum_{c' \neq c} \exp(\hat{\mathbf{w}}_c^\top \hat{\boldsymbol{\mu}}_{c'} / \tau) \right),$$

1018 so that

$$1019 L_{\text{NONL}}^{\text{cls}} = \log n + \tilde{L}_{\text{NONL}}^{\text{cls}}.$$

1020 In what follows we again treat  $(\hat{\boldsymbol{\mu}}_c, \hat{\mathbf{w}}_c)$  as free unit vectors and write  $\boldsymbol{\mu}_c := \hat{\boldsymbol{\mu}}_c$  and  $\mathbf{w}_c := \hat{\mathbf{w}}_c$ .  
 1021

1022 **Step 2: analysis of the class-level problem.** For each class  $c$  we can view the  $c$ th summand in  
 1023  $\tilde{L}_{\text{NONL}}^{\text{cls}}$  as a standard decoupled alignment/uniformity loss of La/Lc type (Koromilas et al., 2024),  
 1024 with:

$$1025 q_c = \mathbf{w}_c \quad (\text{anchor}), \quad k_c^+ = \boldsymbol{\mu}_c \quad (\text{positive}), \quad \{k_c^- = \boldsymbol{\mu}_{c'} : c' \neq c\} \quad (\text{negatives}).$$

1026 The per-class alignment and contrastive terms are  
 1027

$$1028 L_a(q_c, k_c^+) = -\frac{1}{\tau} q_c^\top k_c^+, \quad L_c(q_c, \{k_c^-\}) = \log \left( \sum_{c' \neq c} \exp(q_c^\top k_{c'}^- / \tau) \right).$$

1031 As in the NTCE case,  $L_a$  is strictly decreasing in similarity and  $L_c$  is convex and strictly increasing  
 1032 in the similarities. Therefore we may again invoke the La/Lc minimizer characterization. By The-  
 1033orem 4.1 and Appendix B.1 of Koromilas et al. (2024), provided  $d \geq K$ , the global minimizers of  
 1034  $\tilde{L}_{\text{NONL}}^{\text{cls}}$  over unit vectors satisfy:

- 1035 • **Perfect alignment:**  $\mu_c = w_c$  for all  $c$ .
- 1036 • **Simplex ETF structure:** the directions  $\{\mu_c\}_{c=1}^K$  form a centered regular simplex equiangular  
 1037 tight frame in a  $(K-1)$ -dimensional subspace:

$$1039 \|\mu_c\| = 1, \quad \mu_c^\top \mu_{c'} = -\frac{1}{K-1} \quad \forall c \neq c'.$$

1041 In particular, there exists a simplex ETF  $\{\mu_c\}_{c=1}^K \subset \mathbb{R}^d$  such that  $\mu_c = w_c$  is a global minimizer of  
 1042  $\tilde{L}_{\text{NONL}}^{\text{cls}}$ , unique up to a global rotation and permutation of the class indices.

1044 **Step 3: lifting back to the sample level.** We now relate these class-level minimizers back to the  
 1045 original sample-level NONL objective and derive the NC structure of its global minimizers.

1047 *Existence of Neural Collapse minimizers.* Let  $\{\mu_c\}_{c=1}^K$  be a simplex ETF and set

$$1049 \hat{w}_c := \mu_c, \quad u_i := \mu_{y_i} \quad \text{for all } i.$$

1051 This configuration satisfies NC1–NC3 by construction: within each class  $c$ , all normalized features  
 1052 collapse to  $\mu_c$  (NC1), the vectors  $\{\mu_c\}$  form a centered simplex ETF (NC2), and  $\hat{w}_c = \mu_c$  (NC3).  
 1053 In particular, the feature class means are  $\hat{\mu}_c = \mu_c$ .

1054 Moreover, for this configuration the Jensen inequalities in Lemma A.4 are tight for all  $(c, c')$ : for  
 1055 any anchor class  $c$  and negative class  $c' \neq c$  we have  $\hat{w}_c^\top u_j = \mu_c^\top \mu_{c'}$  for all  $j \in I_{c'}$ , so the negative  
 1056 logits are constant within each negative class. Hence

$$1057 \mathcal{L}_{\text{NONL}} = L_{\text{NONL}}^{\text{cls}}(\{\hat{\mu}_c\}, \{\hat{w}_c\}) = \log n + \tilde{L}_{\text{NONL}}^{\text{cls}}(\{\mu_c\}, \{\mu_c\}).$$

1059 Since  $\{\mu_c\}, \{\mu_c\}$  is a global minimizer of  $\tilde{L}_{\text{NONL}}^{\text{cls}}$ , this shows that

$$1061 \inf_{\{u_i\}, \{\hat{w}_c\}} \mathcal{L}_{\text{NONL}} \leq \log n + \inf_{\{\mu_c\}, \{w_c\}} \tilde{L}_{\text{NONL}}^{\text{cls}}.$$

1064 *Structure of arbitrary global minimizers.* Conversely, let  $(\{u_i^*\}, \{\hat{w}_c^*\})$  be any global minimizer of  
 1065  $\mathcal{L}_{\text{NONL}}$ , and let

$$1066 \hat{\mu}_c^* := \frac{1}{n} \sum_{j \in I_c} u_j^*$$

1068 be the corresponding class means. Lemma A.4 gives

$$1070 \mathcal{L}_{\text{NONL}}(\{u_i^*\}, \{\hat{w}_c^*\}) \geq L_{\text{NONL}}^{\text{cls}}(\{\hat{\mu}_c^*\}, \{\hat{w}_c^*\}) = \log n + \tilde{L}_{\text{NONL}}^{\text{cls}}(\{\hat{\mu}_c^*\}, \{\hat{w}_c^*\}).$$

1072 On the other hand, from the ETF construction above we know that

$$1073 \inf_{\{u_i\}, \{\hat{w}_c\}} \mathcal{L}_{\text{NONL}} \leq \log n + \inf_{\{\mu_c\}, \{w_c\}} \tilde{L}_{\text{NONL}}^{\text{cls}}.$$

1075 Since  $(\{u_i^*\}, \{\hat{w}_c^*\})$  achieves this infimum, the two displays must be equalities. Therefore:

1077 •  $\tilde{L}_{\text{NONL}}^{\text{cls}}(\{\hat{\mu}_c^*\}, \{\hat{w}_c^*\})$  attains the global minimum of  $\tilde{L}_{\text{NONL}}^{\text{cls}}$ , so by the La/Lc minimizer charac-  
 1078 terization we must have, up to a global rotation and permutation of class labels,

$$1079 \hat{\mu}_c^* = \hat{w}_c^* \quad \text{for all } c, \quad \{\hat{\mu}_c^*\} \text{ form a centered simplex ETF.}$$

1080 • Lemma A.4 must be tight at the minimizer, so the Jensen equalities hold for all  $(c, c')$ : for every  
 1081 anchor class  $c$  and negative class  $c' \neq c$ , the logits  $\hat{\mathbf{w}}_c^* \top \mathbf{u}_j^*$  are constant over  $j \in I_{c'}$ , equal to  
 1082  $\hat{\mathbf{w}}_c^* \top \hat{\boldsymbol{\mu}}_{c'}^*$ .

1084 Let  $S := \text{span}\{\hat{\mathbf{w}}_1^*, \dots, \hat{\mathbf{w}}_K^*\}$ , which is the  $(K - 1)$ -dimensional simplex-ETF subspace. Fix a  
 1085 class  $c'$  and  $j \in I_{c'}$ . For every  $c \neq c'$ , tightness of Jensen gives

$$\hat{\mathbf{w}}_c^* \top (\mathbf{u}_j^* - \hat{\boldsymbol{\mu}}_{c'}^*) = 0.$$

1088 As before, since  $\{\hat{\mathbf{w}}_c^*\}_{c=1}^K$  form a centered simplex ETF in  $S$  and  $\sum_{c=1}^K \hat{\mathbf{w}}_c^* = 0$ , any  $K - 1$  of them  
 1089 are linearly independent and thus span  $S$ . In particular, the set  $\{\hat{\mathbf{w}}_c^* : c \neq c'\}$  spans  $S$ , so  $\mathbf{u}_j^* - \hat{\boldsymbol{\mu}}_{c'}^*$   
 1090 is orthogonal to  $S$ , and hence the orthogonal projection of  $\mathbf{u}_j^*$  onto  $S$  equals  $\hat{\boldsymbol{\mu}}_{c'}^*$ .

1092 But both  $\mathbf{u}_j^*$  and  $\hat{\boldsymbol{\mu}}_{c'}^* = \hat{\mathbf{w}}_{c'}^*$  are unit vectors, and  $\hat{\boldsymbol{\mu}}_{c'}^* \in S$ . As in the NTCE case, the only way for a  
 1093 unit vector to have a unit-norm projection onto  $S$  is to lie in  $S$  itself and coincide with its projection,  
 1094 so we must have

$$\mathbf{u}_j^* = \hat{\boldsymbol{\mu}}_{c'}^* \quad \text{for all } j \in I_{c'}.$$

1097 Thus within each class all features collapse to a single unit direction (NC1), these  $K$  directions  
 1098 form a centered simplex ETF (NC2), and the classifier weights align with the class means (NC3).  
 1099 Therefore every global minimizer of  $\mathcal{L}_{\text{NONL}}$  exhibits Neural Collapse, up to a global rotation and  
 1100 permutation of the class labels.

1102 *Proof of Theorem A.1. NormFace:* Lemma A.2 together with Theorem 3.1 of Yaras et al. (2022)  
 1103 shows that every global minimizer of  $\mathcal{L}_{\text{NF}}$  satisfies NC1–NC3.

1105 **NTCE:** Lemma A.3 bounds  $\mathcal{L}_{\text{NTCE}}$  by the class-level loss  $L_{\text{NTCE}}^{\text{cls}}$ , while the La/Lc minimizer  
 1106 characterization (Step 2) identifies the global minimizers of  $\tilde{L}_{\text{NTCE}}^{\text{cls}}$  as simplex ETF configurations  
 1107 with  $\boldsymbol{\mu}_c = \mathbf{w}_c$ . Step 3 shows that any global minimizer of  $\mathcal{L}_{\text{NTCE}}$  must both attain this class-level  
 1108 minimum and satisfy the tightness conditions in Lemma A.3, which enforces NC1. Together these  
 1109 yield NC1–NC3 for all NTCE minimizers.

1110 **NONL:** Lemma A.4 bounds  $\mathcal{L}_{\text{NONL}}$  by the class-level loss  $L_{\text{NONL}}^{\text{cls}}$ , while the La/Lc minimizer  
 1111 characterization (Step 2) identifies the global minimizers of  $\tilde{L}_{\text{NONL}}^{\text{cls}}$  as simplex ETF configurations  
 1112 with  $\boldsymbol{\mu}_c = \mathbf{w}_c$ . Step 3 shows that any global minimizer of  $\mathcal{L}_{\text{NONL}}$  must both attain this class-level  
 1113 minimum and satisfy the tightness conditions in Lemma A.4, which again enforces NC1. Together  
 1114 these yield NC1–NC3 for all NONL minimizers.

1115 In all three cases, the resulting NC configuration is unique up to a global rotation and permutation  
 1116 of the class labels. This proves the theorem.  $\square$

## 1118 A.2 EQUIVALENCE OF SCL AND PROTOTYPE–SOFTMAX MINIMIZERS

1120 Here we provide the proof of Theorem 4.2.

1123 *Proof.* Fix  $i \in [2M]$  with label  $y_i$ . Let  $\mathcal{C}(i) = \{j \in [2M] : j \neq i, y_j = y_i\}$ ,  $\mathcal{B}_c = \{j \in [2M] : y_j = c\}$ ,  
 1124  $n_c = |\mathcal{B}_c|$ , and  $\hat{\boldsymbol{\mu}}_c = \frac{1}{n_c} \sum_{j \in \mathcal{B}_c} \mathbf{a}_j$ .

1125 **(A) SCL lower bound.** By unfolding the SCL loss defined in Equation (2), the per-example loss  
 1126 term can be written as

$$\ell_i^{\text{SCL}} = -\frac{1}{|\mathcal{C}(i)|} \sum_{l \in \mathcal{C}(i)} \frac{\mathbf{a}_i^\top \mathbf{a}_l}{\tau} + \log \sum_{j \in [2M] \setminus \{i\}} \exp(\mathbf{a}_i^\top \mathbf{a}_j / \tau).$$

1131 For the first term, using  $\frac{1}{|\mathcal{C}(i)|} \sum_{l \in \mathcal{C}(i)} \mathbf{a}_l = \frac{n_{y_i} \hat{\boldsymbol{\mu}}_{y_i} - \mathbf{a}_i}{n_{y_i} - 1}$  and  $\|\mathbf{a}_i\| = 1$  gives  
 1132  $-\frac{\mathbf{a}_i^\top}{\tau} \left( \frac{1}{|\mathcal{C}(i)|} \sum_{l \in \mathcal{C}(i)} \mathbf{a}_l \right) \geq -\frac{\mathbf{a}_i^\top \hat{\boldsymbol{\mu}}_{y_i}}{\tau}$ .

1134 For the second term, we group by class, subtract the self term and then apply Jensen classwise due  
 1135 to convexity of the exponential function:

$$1137 \sum_{j \in [2M] \setminus \{i\}} e^{\mathbf{a}_i^\top \mathbf{a}_j / \tau} = \sum_{c=1}^K \sum_{l \in \mathcal{B}_c} e^{\mathbf{a}_i^\top \mathbf{a}_l / \tau} - e^{1/\tau} \geq \sum_{c=1}^K n_c e^{\mathbf{a}_i^\top \hat{\mu}_c / \tau} - e^{1/\tau}.$$

1139 Combining,

$$1141 \ell_i^{\text{SCL}} \geq -\frac{\mathbf{a}_i^\top \hat{\mu}_{y_i}}{\tau} + \log \left( \sum_{c=1}^K n_c e^{\mathbf{a}_i^\top \hat{\mu}_c / \tau} - e^{1/\tau} \right) =: \ell_i^*. \quad (14)$$

1144 Equality in equation 14 holds iff every class-wise sum is collapsed, i.e.,  $\mathbf{a}_j = \hat{\mu}_c$  for all  $j \in \mathcal{B}_c$ ,  
 1145 because the positive-term bound is tight only when  $\mathbf{a}_i^\top \hat{\mu}_{y_i} = 1$  (so  $\mathbf{a}_i = \hat{\mu}_{y_i}$ ) and the classwise  
 1146 Jensen step is tight only when all within-class logits  $\{\mathbf{a}_i^\top \mathbf{a}_l : l \in \mathcal{B}_c\}$  are equal.

1147 **(B) Prototype loss lower bound.** Since  $\mathbf{a}_i^\top \hat{\mu}_{y_i} \leq 1$  for unit vectors,  $e^{\mathbf{a}_i^\top \hat{\mu}_{y_i} / \tau} \leq e^{1/\tau}$ . Therefore

$$1149 \underbrace{\sum_{c=1}^K n_c e^{\mathbf{a}_i^\top \hat{\mu}_c / \tau} - e^{\mathbf{a}_i^\top \hat{\mu}_{y_i} / \tau}}_{=: D_i^{\text{proto}}} \geq \underbrace{\sum_{c=1}^K n_c e^{\mathbf{a}_i^\top \hat{\mu}_c / \tau} - e^{1/\tau}}_{=: D_i^*},$$

1153 and thus, with the *same* numerator  $e^{\mathbf{a}_i^\top \hat{\mu}_{y_i} / \tau}$ ,

$$1155 \ell_i^{\text{proto}} = -\frac{\mathbf{a}_i^\top \hat{\mu}_{y_i}}{\tau} + \log D_i^{\text{proto}} \geq -\frac{\mathbf{a}_i^\top \hat{\mu}_{y_i}}{\tau} + \log D_i^* = \ell_i^*.$$

1156 Averaging over  $i$  gives the following inequalities for any batch  $\mathbf{A}$ :

$$1159 L_{\text{SCL}}(\mathbf{A}) \geq L_*(\mathbf{A}) \\ 1160 L_{\text{proto}}(\mathbf{A}) \geq L_*(\mathbf{A}).$$

1162 **(C) Collapse–simplex makes all three equal.** By Graf et al. (2021, Theorem 2), any SCL global  
 1163 minimizer exhibits class-wise collapse,  $\mathbf{a}_j = \zeta_{y_j}$ , and the directions  $\{\zeta_c\}$  form a centered regular  
 1164 ( $K-1$ )-simplex. Hence  $\hat{\mu}_c = \zeta_c$  and  $\mathbf{a}_i^\top \hat{\mu}_{y_i} = 1$  for all  $i$ , making both inequalities above tight:

$$1165 L_{\text{SCL}}(\mathbf{A}^*) = L_*(\mathbf{A}^*) = L_{\text{proto}}(\mathbf{A}^*).$$

1166 Therefore  $\min L_{\text{SCL}} = \min L_* = \min L_{\text{proto}}$ , all attained at the collapsed-simplex configurations.

1168 **(D) Equality of argmin sets.** Let  $\mathbf{A}$  minimize  $L_{\text{proto}}$ . Then  $L_{\text{proto}}(\mathbf{A}) = \min L_{\text{proto}} = \min L_*$ ,  
 1169 so  $L_*(\mathbf{A}) = L_{\text{proto}}(\mathbf{A})$ , which forces  $e^{\mathbf{a}_i^\top \hat{\mu}_{y_i} / \tau} = e^{1/\tau}$  for every  $i$ , i.e.,  $\mathbf{a}_i^\top \hat{\mu}_{y_i} = 1$  and hence  
 1170  $\mathbf{a}_i = \hat{\mu}_{y_i}$  (class-wise collapse). Moreover  $L_{\text{SCL}}(\mathbf{A}) = L_*(\mathbf{A}) = \min L_{\text{SCL}}$ , so  $\mathbf{A}$  also minimizes  
 1171 SCL.

1172 Graf’s theorem then implies the class means form a centered simplex ETF. Thus the argmin sets of  
 1173  $L_{\text{SCL}}$  and  $L_{\text{proto}}$  coincide (up to rotation and label permutation). □

### 1177 A.3 IMPLEMENTATION DETAILS

1178 Experiments are conducted on four standard image classification datasets: *CIFAR10*, *CIFAR100*,  
 1179 *ImageNet-100*, and *ImageNet1K*, following common representation learning benchmarking practices  
 1180 (Khosla et al., 2020; Markou et al., 2024; Wang et al., 2021; Yeh et al., 2022). We use ResNet50  
 1181 for ImageNet-100/ImageNet1K and ResNet18 for CIFAR10/CIFAR100. All models are trained using  
 1182 SGD optimizer for 500 epochs on ImageNet1K (temperature 0.1) and ImageNet-100 (batch size  
 1183 1024, temperature 0.2) and 1000 epochs on CIFAR10/CIFAR100. For ImageNet1k in order to enable  
 1184 fair comparison we report for each method its best accuracy for training with batch size 2048,  
 1185 4096, and 8192. For CIFAR10/100 we set the batch size to 512 and evaluate all 11 temperatures  
 1186 in the set [0.07, 0.1, 0.2, 0.3, 0.4, 0.5, 0.6, 0.7, 0.8, 0.9, 1]. In Table 1 and Table 2 we report for  
 1187 each method the best performing temperature. For Supervised Contrastive Learning we perform the  
 1188 linear probing phase for the typical 90 epochs.

1188 A.3.1 CLASSIFIER LEARNING METHODS (CE, NORMFACE, NTCE, NONL)  
11891190 For the family of classifier learning methods, we employ the following hyperparameters across  
1191 datasets:  
11921193 **CIFAR10/CIFAR100.** Models are trained for 1000 epochs with batch size 512. We use SGD  
1194 optimizer with momentum 0.9, weight decay  $10^{-4}$ , and initial learning rate 0.2. The learning rate  
1195 follows a cosine annealing schedule throughout training, decaying to a minimum value of  $\eta_{\min} =$   
1196  $\eta_0 \times 0.1^3$  where  $\eta_0$  is the initial learning rate. Data augmentation consists of RandomResizedCrop  
1197 with scale (0.2, 1.0), RandomHorizontalFlip, and standard normalization with dataset-specific mean  
1198 and standard deviation values.  
11991200 **ImageNet-100.** ResNet50 models are trained for 500 epochs with batch size 1024 (256 per GPU  
1201 with 4 GPUs). We employ SGD optimizer with momentum 0.9, weight decay  $10^{-4}$ , and initial  
1202 learning rate 0.1, which is automatically scaled based on the total batch size. We use cosine an-  
1203nealing scheduler with 10 epochs of linear warmup from 0.01 to the target learning rate. After  
1204 warmup, the learning rate follows a cosine decay to  $\eta_{\min} = \eta_0 \times 0.1^3$ . Synchronized BatchNorm is  
1205 enabled across GPUs. Data augmentation includes RandomResizedCrop(224) with scale (0.2, 1.0),  
1206 RandomHorizontalFlip, and standard ImageNet normalization.  
12071208 **ImageNet1K.** ResNet50 models are trained for 500 epochs with batch size 2048 (256 per GPU  
1209 with 8 GPUs). Hyperparameters follow the same configuration as ImageNet-100, with SGD opti-  
1210 mizer (momentum 0.9, weight decay  $10^{-4}$ ), initial learning rate 0.1 with automatic scaling based on  
1211 batch size. We apply 10 epochs of linear warmup followed by cosine annealing to  $\eta_{\min} = \eta_0 \times 0.1^3$ .  
1212 Data augmentation and normalization follow ImageNet-100 settings.  
12131214 A.3.2 SUPERVISED CONTRASTIVE LEARNING  
12151216 For supervised contrastive methods, we implement a two-phase training procedure:  
12171218 **Phase 1: Contrastive Training.**  
12191220 **CIFAR10/CIFAR100:** Models are trained for 1000 epochs with batch size 512. SGD optimizer  
1221 is used with momentum 0.9, weight decay  $10^{-4}$ , and initial learning rate 0.05. The learning rate  
1222 follows cosine annealing schedule throughout training, decaying to  $\eta_{\min} = \eta_0 \times 0.1^3$ . We use  
1223 extensive data augmentation including RandomResizedCrop with scale (0.2, 1.0), RandomHorizontal-  
1224 Flip, ColorJitter(0.4, 0.4, 0.4, 0.1) with probability 0.8, and RandomGrayscale with probability  
1225 0.2. Each image generates two augmented views for contrastive learning.  
12261227 **ImageNet-100:** ResNet50 encoder with 128-dimensional projection head is trained for 500 epochs  
1228 with batch size 1024. We use SGD optimizer with momentum 0.9, weight decay  $10^{-4}$ , and base  
1229 learning rate 0.8 (automatically scaled by batch size). Learning rate follows cosine annealing with  
1230 10 epochs linear warmup from 0.01, then decays following a cosine schedule to  $\eta_{\min} = \eta_0 \times 0.1^3$ .  
1231 Data augmentation extends CIFAR settings with the addition of Gaussian blur for ImageNet scale  
1232 images.  
12331234 **ImageNet1K:** Training spans 500 epochs with batch size 2048 using the same optimizer configu-  
1235 ration as ImageNet-100. Base learning rate is set to 0.1 with automatic scaling. We employ cosine  
1236 annealing with 5 epochs warmup from 0.01, followed by cosine decay to  $\eta_{\min} = \eta_0 \times 0.1^3$ . The  
1237 same augmentation pipeline as ImageNet-100 is used.  
12381239 **Phase 2: Linear Evaluation.** For all datasets, we freeze the learned encoder and train a linear  
1240 classifier on top of the representations:  
12411242 **CIFAR10/CIFAR100:** Linear classifier is trained for 100 epochs using SGD with learning rate 5.0,  
1243 momentum 0.9, and zero weight decay. Learning rate is decayed by factor 0.2 at epochs 60, 75, 90  
1244 using a step scheduler.  
12451246 **ImageNet-100:** Linear evaluation runs for 90 epochs with SGD optimizer, learning rate 2.0, mo-  
1247 mentum 0.9, and zero weight decay. Learning rate decay by factor 0.2 occurs at epochs 30, 60, 80  
1248 using a step scheduler.  
1249

1242 **ImageNet1K:** Linear classifier training spans 90 epochs with SGD, learning rate 0.8, momentum  
 1243 0.9, and zero weight decay. The same step decay schedule as ImageNet-100 is applied.  
 1244

1245 **A.3.3 ADDITIONAL IMPLEMENTATION DETAILS**  
 1246

1247 For distributed training on ImageNet datasets, we employ `DistributedDataParallel` with one process  
 1248 per GPU. Random seed is fixed at 42 for reproducibility. The cosine annealing scheduler is imple-  
 1249 mented following the standard formulation:  $\eta_t = \eta_{\min} + \frac{1}{2}(\eta_0 - \eta_{\min})(1 + \cos(\frac{\pi t}{T}))$ , where  $t$  is  
 1250 the current epoch and  $T$  is the total number of epochs. For experiments with warmup, the warmup  
 1251 period linearly interpolates from the warmup starting learning rate to the initial learning rate before  
 1252 transitioning to cosine annealing. Temperature parameter  $\tau$  is searched over the range [0.07, 0.1,  
 1253 0.2, ..., 1.0] for CIFAR experiments, while ImageNet experiments use the optimal temperature found  
 1254 through preliminary experiments (0.1 for supervised contrastive, 0.2 for classifier learning methods).  
 1255 All models use standard weight initialization and no additional regularization beyond weight decay.  
 1256

1257 **A.4 EXTRA ABLATION STUDIES**  
 1258

1259 **A.4.1 ROLE OF THE PROJECTION HEAD**  
 1260

1261 **Table 7: Contrastive Learning Results - Without Projection Head.** Performance comparison  
 1262 across different classifier learning approaches without projection head.  
 1263

1264 <b>Classifier Learning</b>	1265 <b>Loss</b>	1266 <b>CIFAR-10</b>	1267 <b>CIFAR-100</b>	1268 <b>ImageNet-100</b>	1269 <b>ImageNet-1K</b>
1266 LINEAR PROBING	1267 SCL	1268 95	1269 70.6	1270 84.1	1271 71
1268 NORMALIZED LINEAR PROBING	1269 SCL	1270 95	1271 71.4	1272 84.3	1273 72.1
1270 FIXED PROTOTYPES	1271 SCL	1272 95	1273 71.4	1274 84.7	1275 70.1

1272 In Table 7 we demonstrate the importance of the projection head in contrastive training. Across three  
 1273 datasets, except on the relatively simple CIFAR-10 benchmark, removing the head consistently re-  
 1274 duces accuracy by more than 2 points. At first glance, one might expect the opposite: discarding the  
 1275 head should let the loss act directly on the final encoder embeddings on the unit hypersphere. We  
 1276 hypothesize that the projection head helps primarily by imposing a beneficial dimensionality bot-  
 1277 tleneck. With ResNet-50, the encoder’s representation is 2048-dimensional, whereas the projection  
 1278 head maps it to 128 dimensions. For a  $K$ -class problem (e.g.,  $K = 100$ ), the ideal equiangular tight  
 1279 frame (ETF) geometry lives in a  $(K - 1)$ -dimensional subspace. Encouraging embeddings to adopt  
 1280 this structure is plausibly easier in a 128-dimensional space than in a 2048-dimensional one, where  
 1281 the optimizer has many more irrelevant directions to explore.  
 1282

1283 **A.4.2 EFFECTIVE HYPERPARAMETER RANGES**  
 1284

1285 Normalized softmax losses introduce two hyperparameters that originate from contrastive learning (i)  
 1286 temperature, and (ii) need for larger batch size. Here we test whether and how these hyperparameters  
 1287 affect the downstream performance.

1288 We conduct hyperparameter optimization experiments on CIFAR-10 and CIFAR-100, evaluating all  
 1289 combinations of 11 temperatures in the range [0.07, 1] and 7 batch sizes in the range [32, 2048].  
 1290 The results show that different contrastive learning methods exhibit distinct optimal hyperparameter  
 1291 regions with minimal overlap in their peak performance zones across both datasets.

1292 In Figure 1 we can see that normalized softmax losses exhibit the same behavior in terms of down-  
 1293 stream performance compared to self-supervised contrastive learning (Chen et al., 2020), which  
 1294 means that there are trustable goto to setups for instance  $\tau = \{0.1, 0.2\}$  for small to medium num-  
 1295 ber of classes datasets and  $\tau = \{0.07, 0.1\}$  for large. For that reason normalized softmax methods  
 despite introducing extra hyperparameters, this is not a problem in practice

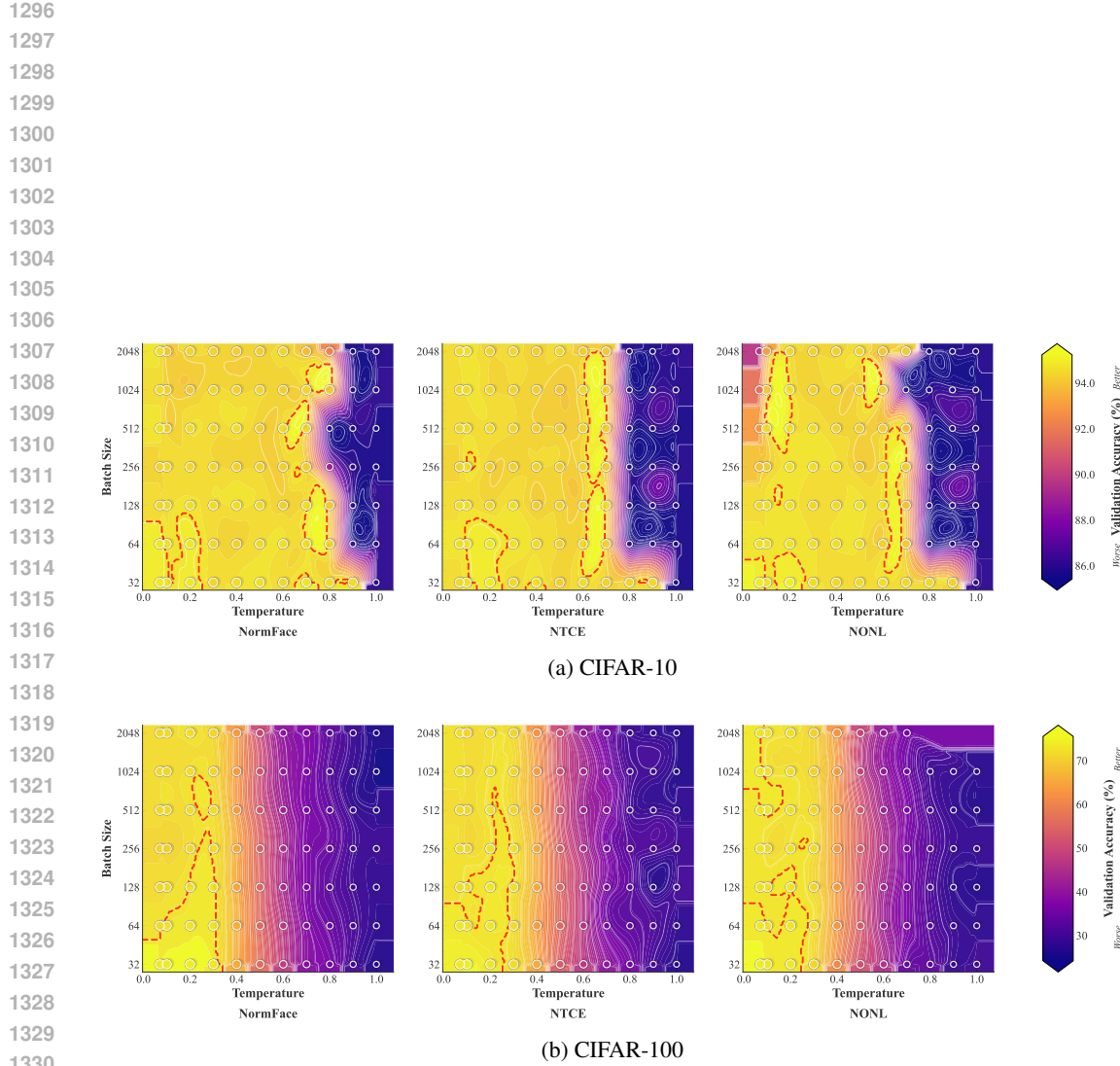


Figure 1: **Validation Accuracy (%) Phase Diagrams.** Classification accuracy on validation set. Higher values indicate better generalization performance. Each subplot shows the performance landscape across temperature and batch size hyperparameters for different loss functions: NormFace, NTCE, and NONL. Brighter regions indicate superior performance. White contour lines indicate iso-performance curves for detailed analysis. Red dashed contours highlight optimal parameter regions (top 10% performance). Scatter points represent individual experimental runs with performance-based sizing. Each dataset uses its own optimal colorbar range. Results originate from grid runs across temperature values in [0.07, 1.0] and batch sizes in 32, 64, 128, 256, 512, 1024, 2048.

Loss	2048	4096	8192
CE	75.4	75.4	75.1
NORMFACE	75.6	76.4	76.3
NTCE (ours)	<b>76.0</b>	<b>76.7</b>	<b>76.7</b>
NONL (ours)	75.0	76.2	76.5

Table 8: Top-1 accuracy (%) on ImageNet-1K for different batch sizes and loss functions.

Table 9: ImageNet-100 top-1 accuracy (%) for different backbones. Best results per column are highlighted in **green**. The last row reports the relative improvement of NONL over CE.

Method	ResNet-50	ResNet-101	ResNet-152	Mean
CE	84.4	85.3	85.5	<b>85.1</b>
NormFace	84.4	85.4	85.6	<b>85.1</b>
NTCE	84.7	85.4	85.4	<b>85.2</b>
NONL	<b>84.9</b>	<b>85.5</b>	<b>85.8</b>	<b>85.4</b>
$\Delta(\text{NONL}-\text{CE})$	+0.6%	+0.2%	+0.4%	<b>+0.4%</b>

#### A.4.3 EFFECTIVE HYPERPARAMETER RANGES

Normalized softmax losses introduce two hyperparameters inherited from contrastive learning: the temperature  $\tau$ , which controls the sharpness of the similarity distribution, and the need for larger batch size  $B$ , which governs the number of in-batch negatives. We assess their impact by grid-searching  $\tau \in [0.07, 1.0]$  (11 values) and  $B \in \{32, 64, 128, 256, 512, 1024, 2048\}$  on CIFAR-10 and CIFAR-100 with NormFace, NTCE, and NONL.

Figure 1 shows consistent “sweet spots” across methods: accuracy forms a pronounced band at moderate temperatures, with performance degrading for overly large  $\tau$  and, to a lesser extent, for very small  $\tau$ . The location of this band shifts toward slightly smaller temperatures as the number of classes increases (CIFAR-100 vs. CIFAR-10), mirroring observations in self-supervised contrastive learning (Chen et al., 2020). Within the effective temperature range, performance is comparatively insensitive to  $B$ , yielding a broad plateau over batch sizes—large batches can help, but are not strictly required.

In practice, these trends provide the same reliable defaults as in self-supervised contrastive learning (Chen et al., 2020):  $\tau \in \{0.1, 0.2\}$  works well for small- to medium-class datasets, while  $\tau \in \{0.07, 0.1\}$  is preferable for larger-class settings. Thus, although normalized softmax losses expose additional hyperparameters, their effective ranges are narrow and stable, so a small amount of tuning (or even these defaults) is typically sufficient to reach near-peak accuracy.

#### A.5 NEED FOR LARGE BATCH SIZE

#### A.6 APPLICABILITY TO LARGER ARCHITECTURES

#### A.7 TRAINING DYNAMICS

In Figure 2 the training dynamics are demonstrated. While cross-entropy (CE) achieves perfect training accuracy, it fails to reach neural collapse geometry, plateauing at suboptimal metric values. CE’s accuracy improvements appear to *derive solely from magnitude and bias adjustments* rather than geometric reorganization. In contrast, our methods *simultaneously optimize all NC metrics throughout training*, converging to proper NC geometry while maintaining optimal accuracy.

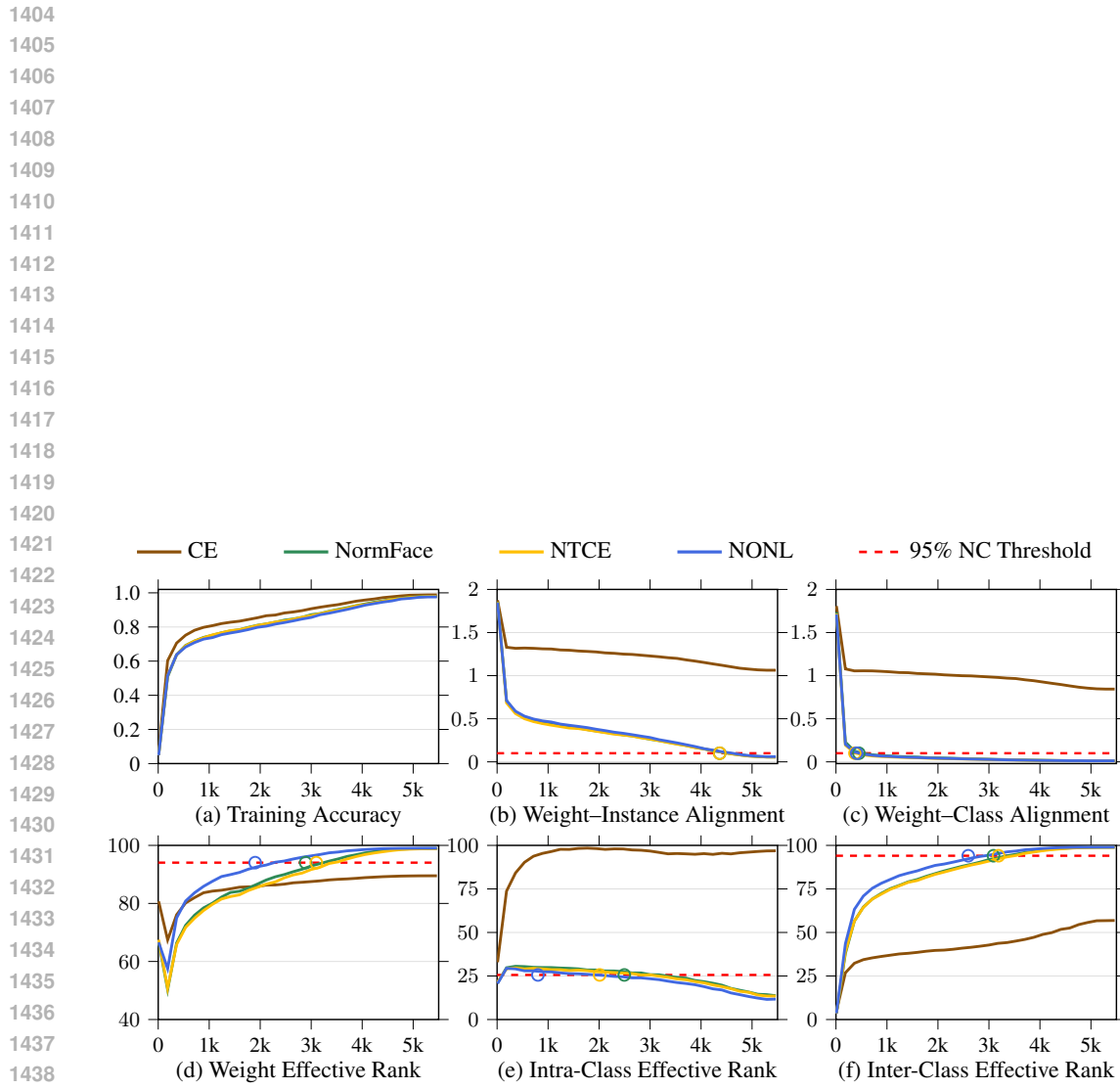


Figure 2: **NC convergence on CIFAR-100.** Six metrics vs. training iterations; red dashed lines mark the 95% NC threshold and circles denote each method's convergence.